Experimental exploration of volcanic rocks-atmosphere interaction under Venus surface conditions

Gilles Berger, Annick Cathala, Sébastien Fabre, Anastassia Yu. Borisova, Alain Pages, Thierry Aigouy, Jerôme Esvan, Patrick Pinet

EXPERIMENTAL EXPLORATION OF VOLCANIC ROCKS-ATMOSPHERE INTERACTION UNDER VENUS SURFACE CONDITIONS

Gilles Berger[1], Annick Cathala[1], Sébastien Fabre[1], Anastassia Y. Borisova[2,3], Alain Pages[1], Thierry Aigouy[2], Jerôme Esvan[4], and Patrick Pinet[1]

[1] IRAP, Université Paul Sabatier, CNRS, 14 avenue E. Belin, 31400 Toulouse, France.

[2] GET, Université Paul Sabatier, CNRS, 14 avenue E. Belin, 31400 Toulouse, France.

[3] Geological Dept., Lomonosov Moscow State University, Vorobievy Gory, Moscow, Russia

[4] CIRIMAT, CNRS-UPS-INPT, ENSIACET, 4 allée Emile MONSO, 31030 Toulouse, France

corresponding author : G. Berger, gilles.berger@irap.omp.eu , +33 56133 2582

Declarations of interest: none

Keywords : Venus surface; Alteration; Experimental; Gas transfer

Highlights:

- Samples were altered at 475°C, typically 1 week and 90bars, in Venus-like gas
- Only olivine and glasses show signs of oxidation/alteration
- In dry gas, olivine is coated by Fe-oxides and glass is oxidized (magnesioferrite)
- Ca, Na, Mg, were transferred from glass to the gas phase or mineralized as sulfate
- In wet gas (early Venus) glass alteration rate is modeled by a shrinking core model

Graphical Abstract

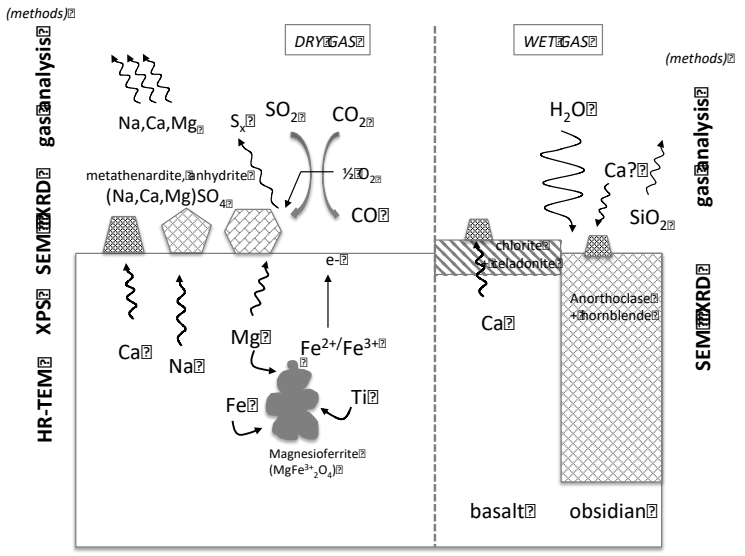

Abstract

This study presents an inventory of possible chemical reactions affecting, or having affected, the Venus surface. Fluid rock reactions are simulated using experiments under conditions close to the present surface. Slabs or powder of several natural and synthetic silicate material (crystalline fresh basalt, altered basalt, obsidian, pumice and basalt glass) were reacted at 475°C in CO_2-H_2O-H_2S-SO_2-CO gas mixture. Most of the runs were carried out at roughly 90 bars with a duration of one week, some experiments having longer (one month) or shorter (one day) durations. The role of H_2O content was explored through a wide range of water pressure: from dry gas for the current Venus conditions up to 590 bars (86%H_2O) for early Venus (or other early terrestrial planets). The gas phase was sampled before the completion of the runs for chemical analysis of major gas components (CO, H_2S, SO_2) as well as trace elements possibly released by the rocks. The altered samples were examined by a suite of mineralogical and chemical techniques (scanning and transmission electron microscopy, X-ray diffraction and spectroscopy).

In dry atmosphere, the redox potential of the gas was close to the Ni/NiO buffer (-21.3 to -27.3 log fO_2), thus close to the current Venus conditions. The sample alteration is tenuous and limited to surface oxidation of glasses and coating of olivine by iron oxides, as well as the general deposition of $(Ca,Na)SO_4$ at the sample surface. The oxidation of glass is reflected in the formation of magnesioferrite under the surface and is accompanied by the release of Ca, Mg and Na into the gas phase or mineralized as sulfate at the surface. In wet atmosphere, obsidian recrystallizes into a mixture of plagioclase and amphibole while basaltic glass produced non-expandable clays minerals: chlorite-type (2:1:1) at the surface and likely celadonite (2:1) below the surface. Olivine is preserved. Using obsidian (the most alterable material) as a proxy of aluminosilicates, we discuss the surface reactions operating under supercritical conditions, and we used a shrinking-core equation for modeling the long-term reactions.

These parametric exploration offer new insights into processes having affected the surface of Venus and contribute to the discussion of open questions such as the fate of water or the lifetime of vitreous dust or fine grain material if present in the current or past Venusian environment. Longer duration experiments will provide more kinetic parameters that can be extrapolated to the geologic history of Venus.

1. Introduction

Modern Venus is considered as a hot and dry planet with a dense carbon dioxide atmosphere. Its surface with an average atmosphere temperature of ~470°C has been shaped within the geologically recent past by a volcanic activity resulting in the formation mostly of basaltic rocks. The predominant basaltic composition of Venus' plains was determined by X-ray fluorescence and Gamma-ray spectrometry during the landing site of Venera 13-14 and Vega 2 space missions (Surkov *et al.*, 1984, 1986), while Venera 8 sampled materials which resemble alkaline rocks (Surkov *et al.*, 1987). In addition, near infrared windows explored by remote sensing suggest that the lower emissivity of tesserae terrain may be interpreted as felsic composition (Hashimoto *et al.*, 2008; Gilmore *et al.*, 2017). Although the absence of plate tectonics suggests that the petrology of Venus's surface is basaltic, its detailed mineralogy is still a matter of debate. For Mars for example, another terrestrial planet without plate tectonics, differentiated rocks were discovered in the Gale crater (Sautter *et al.*, 2015).

The deep atmosphere at contact with the surface contains small amounts of sulfur-bearing species and trace amounts of H_2O contents. The well-known low dielectric constant of CO_2 and the low water concentration, roughly 30 ppm, preclude *a priori* extensive alteration of the volcanic rocks, at least in the present day conditions. But several morphologic and chemical features of the Venusian soil, however, suggest that the volcanic material has undergone chemical interaction with the atmosphere. Among them, reflectance spectra measured at the Venera 9-10 landing sites (Ekonomov *et al.*, 1980) match with hematite (Pieters *et al.*, 1986), which is uncommon in unaltered basalts under dry conditions. Comparison with the bulk-rock analysis suggests an enrichment of the surface rocks in Fe^{3+}-bearing material (Shkuratov *et al.*, 1987). The experimental study by Fegley *et al.* (1995) on pyrite decomposition supported this observation. Oxidation by SO_2 content in the deep atmosphere is an alternative as demonstrated by Radoman-Shaw *et al.* (2017) based on wollastonite, used in their study as a proxy for Ca-silicates. It is interesting to note that the other Ca-bearing silicates tested in this study did not show an equivalent sulfurization of the surface even after 42 days of reaction.

Understanding the degree of rock-atmosphere interaction is crucial for both the composition of atmosphere and the Venus surface, in particular for the cycle of sulfur and water. For example, rock alteration products enriched in sulfates (anhydrite) are expected to control the complex sulfur cycle on Venus (Fegley and Prinn, 1989; Zolotov, 2007, 2008, 2018). However, thermodynamic predictions involving anhydrite underestimate the current SO_2 content of Venus atmosphere (Sidorov, 2006; Treiman and Schwenzer, 2009) suggesting that SO_2 is not entirely buffered by atmosphere-surface chemistry (Gilmore *et al.*, 2017). The relative stability of sulfide and sulfate, under deep Venus atmosphere is also an issue and is reviewed by Zolotov (2018). The formation of sulfide is expected at highlands and may contribute to the low radar emissivity above 2-4 km, although atmospheric data does not clearly demonstrate this assumption. Similarly, the fate of water through the geological

history of Venus is still unclear: how hydrated are (or may have been) the basaltic rocks exposed at the surface? What was the contribution of rock hydration versus atmospheric escape from the early atmosphere for the H_2O budget? Venus, although similar to Earth in many aspects, did not undergo a comparable geodynamical evolution (no plate tectonics). This important question in comparative planetology may be related to water abundance in the Venus crust – as water is well known to modify the petrophysical properties - and more generally the Venus water cycle (Smrekar and Sotin, 2012, Taylor *et al.*, 2018). From thermochemical calculations, all hydrated minerals and the majority of OH-bearing minerals are unstable today at the Venus surface (Zolotov et al., 1997), although oxyamphiboles may be metastable as suggested by Straub and Burns (1993). The recent review by Gilmore *et al.* (2017) discussed several scenarios of atmospheric H_2O variation with time and their relationships with formation of tesserae tectonic region. The hypotheses range from a rapid early decline to a more recent but sporadic decline, the latter being associated to sporadic influx from recent volcanism. Recent volcanism may have enabled gas-solid-type alteration reactions, admittedly in restricted area and time interval, under environmental conditions similar to those today. The surface rock-atmosphere reaction may be also important to understand the highlands radar anomalies that may be attributed to high-ε semi-conductor materials (Gilmore *et al.*, 2017).

Improved knowledge of mechanisms and rates of rock-gas interaction in Venus's present or past atmospheric conditions is required to better constrain the evolution of both the surface and atmosphere with time. Thermodynamic calculations in dry actual atmosphere (Zolotov et al., 1997) predicted the formation of iron oxides and sulfate, even enstatite from olivine. In wet atmosphere, serpentinization of olivine or the green schist facies albite-epidote-chlorite for basalt is expected. However, the kinetic constraints of gas-rock systems are not trivial and are challenging in our case. Alteration kinetics of silicate minerals has been extensively investigated in the last decades in aqueous solution below the water critical point, i.e. a condensed polar liquid (dielectric constant > 20). Under the extreme conditions of deep Venus atmosphere, and in a CO_2-dominated gas, theoretical and experimental studies are rare. The study by Zhang *et al.* (2011) explored the rate and stoichiometry of dissolution of actinolite and pyroxene in water above 300°C, at conditions when the density and the dielectric constant of the fluid decrease causing the destruction of the water molecules' hydrogen bond network and so affecting the rates of ionic reactions and hydration of the silicate framework. The consequence is that the kinetics of silicate dissolution in the subcritical and supercritical region is not well described by an Arrhenius form, as it is the case at lower temperature. Zhang *et al.* (2011) proposed a kinetic expression integrating the effect of the dielectric constant where the logarithm of the rate decrease is inversely correlated to the inverse of the dielectric constant. In CO_2 fluids, the dissolution of silicate phases is even less documented, at least in pure CO_2, because the very low dielectric constant of such non-polar fluids makes it quite unlikely to breakdown the silicate structure despite favorable Gibbs free energy of reaction. Few studies are available in the literature on the subject. A recent review of gas-rock interaction at high temperature by King *et al.* (2018) presents an inventory of chemical

reactions occurring between SO_2 and silicate minerals or glasses with geologic examples. Under dry atmosphere, SO_2 is considered as an alternative to H_2O for silicate alteration. Details of the reactions are discussed in Renggli *et al.* (2018), Palm *et al.* (2018), King *et al.* (2018) and Delmelle *et al.* (2018). Applied to Venus, the expected reaction is surface oxidation and sulfate growth (Zolotov, 2018; King *et al.*, 2018).

Most theoretical studies on Venus surface-atmosphere interaction focus on the modern dry conditions. The impact of atmospheric water during its early history, or during more possibly recent wet, volcanic events, are not documented although small content of water may significantly change the processes. At lower temperature for example, the rare studies devoted to the silicate alteration in CO_2 suggest that the observed alterations were driven by few % H_2O in the gas, either because the gas phase was equilibrated with an aqueous solution (Daval *et al.*, 2009) or because the starting minerals were hydrated (Regnault *et al*., 2009). In order to address the role of H_2O on these reactions, and more generally to elucidate the chemical and mineralogical processes operating under the specific conditions of Venus, we conducted an experimental program covering the present day conditions. We have reacted a variety of crystallized and vitreous silicate rocks in a CO_2-dominated atmosphere, with variable amounts of H_2O and sulfur species, and under typical current conditions of Venus surface: 470°C, ≈100 bars. Most of the experiments were conducted for roughly one week (~ 170 hours) except some tests which ran from 1 day (24 hours) to 1 month (~720 hours). We have tested the consequence of the presence of sulfurized gaseous species by comparing runs of pure CO_2 with runs of sulfurized CO_2. The effect of H_2O was investigated using dry to water-dominated gas and up to 590 bars vapor pressure. Among the rock samples, glasses of several compositions were used. Even if vitreous materials are not the most representative materials of Venus surface, they may have been produced in pyroclastic flows as those recently described in Campbell *et al.* (2017). The mineralogical signatures of the experimental sample products were analyzed at the end of the runs by scanning and high resolution transmission electron microscopy (SEM, HR-TEM), X-ray diffraction (XRD) and X-ray photoelectron spectroscopy (XPS), while aliquots of gaseous phase were sampled during the course of experiments and analyzed for their chemical composition. In addition to direct implications for the rock-atmosphere interaction on Venus, this study also discusses the mechanisms and rates of silicate alteration at high temperature in a low-density supercritical fluid rich in CO_2 or CO_2-H_2O mixture.

2. Experimental procedure

2.1 Experimental design

The experiments were conducted at 475°C in an Autoclave-France® bolt-closure reactor made of Hastelloy-C276. This Ni-based alloy (59%Ni, 17%Cr, 16%Mo, 5%Fe, 3%W) prevents corrosion of the reactor in aggressive media such as CO_2-H_2S/SO_2-H_2O mixture, although a sulfidation of Hastelloy may occur at high temperature in presence of SO_2 (Tu and Goto, 2005). The internal volume

of the reactor is 320 mL and measures 48x190 mm. The vessel is equipped with several connections (in H-C276) that enabled sampling of the fluid phase during the run and/or injection of gas or liquid. The tightness between the body and head of reactor is ensured by a metallic gasket sealed with an additional 0.2 or 0.5 mm thick graphite sheet. The temperature was held constant by a West@6100 PID controller attached to an electric collar-type heater within nominally 1°C for a dense solution (aqueous liquid). A more complete description of the device can be found in Savary et al. (2012). The vessel was initially designed for aqueous solutions and was equipped with an impeller driven by an external magnetic driver to homogenize the temperature and fluid chemistry. With supercritical fluids at low density (typically 0.08-0.15 in the present case), the thermal regulation by the impeller was less efficient, with variations up to 3°C, and we finally removed it to simply the design. The rock samples were accommodated in a 25mm high x 20mm diameter Pt-crucible fixed at half-height of the reactor body adjacent to an internal J thermocouple.

2.2 Rock samples

The three rock samples and three synthetic vitreous materials that were used are briefly described below. They were selected to cover a large range of rock composition and geological context. The bulk chemical compositions of the starting samples and minerals of interest of the crystallized rocks are reported in Table 1.

Millimeter-length beads of four rock samples were selected after grinding massive samples. These beads were dedicated to the investigation of the altered surface by microscopic observations. The origin and description of the four starting rocks is listed thereafter:

- A picritic basalt from the 2007 eruption of Piton de la Fournaise, Réunion Island, western Indian Ocean, was selected for the investigation of the behavior of individual mineral, in particular olivine. The basalt contains millimetric phenocrysts of olivine (80%Fo), sub-millimetric crystals of augite, labradorite and magnetite embedded in a cryptocrystalline matrix.
- A basaltic pumice collected in 1990 in a fresh lava flow of the Pu'u'O'o volcano, Kilauea, Hawaï, represents a standard volcanic glass. It is vitreous, unaltered and contains mineral inclusions of augite and labradorite.
- A natural unaltered vitreous obsidian, collected at Vulcano Island, Italia, was selected to test the behavior of glasses having a chemical composition that differs from that of a standard basalt. The lava contains millimeter-length elongated vacuoles covered by spherical aggregates (lepidosphere) of opaline silica. The bulk composition is intermediate between trachyte and rhyolite.
- The natural vitreous materials were completed by a synthetic alkaline glass. It was prepared for a previous study and details are available in Berger *et al.* (1994).

In addition to the beads, some samples were conditioned in other forms for specific purpose:

- We prepared a powder from a tholeitic basalt from Pic d'Ysson, Massif Central, France. This sample is a fine grain basalt and was used in a previous study (Souchon *et al.*, 2011). The 100-150 μm sized fraction was selected by sieving and was ultrasonically cleaned. Its specific surface area measured by nitrogen or krypton gas adsorption (BET method) is 1.2 m^2g^{-1}. It is very slightly altered as shown by its 0.8% H_2O content, a high specific surface area and the presence of rare alteration features observed under SEM. The high surface area of this sample was supposed to enhance the chemical transfer (if any) from the basalt towards the atmosphere.
- We also prepared a fine powder of a natural altered basalt collected at contact with the quartz-syenite intrusion constituting the Piton des Neiges, Réunion Island. An accurate description is given in Berger *et al.* (2018). It is composed of clinopyroxene (diopside), plagioclase (andesine) and monomineralic corrensite (1:1 regular intercalation of trioctaedral chlorite-smectite). This clay-rich sample was dedicated to the monitoring of the crystallographic changes of the clay fraction by XRD.
- Polished slides of the synthetic alkaline basaltic glass (10x10x1mm) were dedicated to XPS analysis of the altered surface.
- Finally, the synthetic alkaline glass was conditioned in powder to increase the reactive surface area. We selected the 125-250 μm fraction. Its specific surface area measured by BET is 0.031 m^2g^{-1} after ultrasonic cleaning. In one run we used a fine crushed powder (< 50 μm, 0.143 m^2g^{-1}) to even more increase the surface area exposed to alteration.

Sample	SiO_2	Al_2O_3	Fe_2O_3(t)	CaO	MgO	Na_2O	K_2O	TiO_2	MnO	H_2O
obsidian	73.1	13.4	2.3	1.03	0.19	4.19	5.25	0.11	0.08	0.54
alkaline basaltic glass	49.0	16.7	11.5	7.18	4.69	3.99	2.34	2.86	0.15	0.14
tholeitic glass slide	40.2	11.1	13.1	10.4	13.1	3.5	1.5	2.5	0.3	
basaltic pumice	48.9	14.3	12.3	11.2	6.52	2.75	0.79	2.83	0.17	0.18
altered basalt										
bulk	44.1	12.4	12.8	8.90	9.56	2.73	0.11	2.10	0.18	3.16
corrinsite (*)	35.1	13.7	15.2	0.90	22.4	12.2	-	0.1	-	12.2
Cpx (*)	50.4	3.8	5.2	21.1	15.7	0.2	-	-	0.2	-
picritic basalt										
olivine (*)	37.8	0	17.8	0.4	43.0	-	-	-	-	
pyroxene (*)	48.8	3.3	8.8	28.4	15.7	-	-	-	-	
tholeitic basalt	43.4	12.1	11.8	9.63	14.1	3.19	1.43	2.35	0.18	0.80

***Table 1**: Composition of starting materials. The bulk compositions were analyzed by the Analytical Research Facility of the CRPG, Nancy, France. (*) The individual minerals were analyzed on polished section by energy dispersive spectroscopy (EDS) under SEM.*

2.3 Gas loading

Three gas systems were tested: (i) pure CO_2, (ii) Venus-like atmosphere (CO_2 with 3.5%N_2 and traces of CO, H_2S and SO_2), and (iii) a mixture of each gas with H_2O. Before loading the reactor with the desired gas, it was flushed with argon to remove any trace of oxygen. The amount of loaded gas

was calculated at the temperature of loading using Equation of State (EOS) models (Duan *et al.*, 1995; Bakker, 2009).

(i) For pure CO_2, we used commercially purified gas at grade 4.5, at approximately 48bar. After heating, the final pressure was adjusted to 90bar by decompressing the excess of pressure if necessary.

(ii) For the Venus-like gas we used a feed bottle of CO_2-based gas mixture at a pressure of 28 bars, the maximum pressure to avoid an incongruent condensation of a liquid phase at low temperature. The reactor was then adjusted to 50 bar using pure CO_2, the feed Venus gas bottle having concentrations in N_2 and SO_2 twice to the nominal values (7% N_2, 30ppm CO, 6ppm H_2S, 260ppm SO_2). Preliminary runs showed that the sulfurized species reacted with Hastelloy and decreased with time. To prevent this artefact we proceeded to a preventive sulfurization of the reactor consisting of heating elemental sulfur in a wet atmosphere. At high temperature the hydrolysis and disproportionation of sulfur provides sulfide and sulfur oxides that saturate the reactor surface. Thus, H_2S and SO_2 are released during the runs at a concentration level that is not exactly the present-day concentration of Venus deep atmosphere but that allows us to evaluate the importance of these species in the surface-atmosphere interaction. The gas mixture containing H_2S, SO_2 and CO was monitored at the end of each run during the decompression stage with a Micro5 detector commercialized by BW-Technologies©. The typical concentration range was 11-68ppm H_2S, 25-688ppm SO_2 and 17-500ppm CO. The high content of CO results from the reaction of CO_2 with graphite used for the gasket sealing. In the last run using dry Venus-like gas we enriched the gas mixture with 2% CO in order to test a possible metal transportation as carbonyl species, as suggested by Simakin *et al.* (2016).

(iii) For the wet gas experiments, variable amounts of pure water were injected in the reactor by an HPLC pump once the temperature and pressure with the dry gas were stabilized. The pressure increased proportionally to the mass of injected water. However, the final pressure was systematically lower, down to 25%, than the expected pressure as predicted with EOS models. This difference, not observed with dry gas, is likely the consequence of colder zones in the system where water may progressively condensate when fH_2O increases (the bottom of the reactor body and the head equipped with the connections are outside of the heating collar). We finally calculated the water fugacity in the gas mixture from EOS models (Duan *et al.*, 1995; Bakker, 2009).

2.4 Procedure and analytical methods

Several rock samples were tested simultaneously in the Pt-crucible. Tables 2 and 3 present the conditions of each experiment. The gas was left to react with the rock samples for one to two weeks in most cases. The gas pressure decreased sometimes with time due to leakage of the system, in particular in the first runs. For these runs, we reported in the table the minimal and maximal values of the pressure range. At the end of the runs the gas was sampled three consecutive times at the temperature of the run in a dedicated 15 mL closed cell made of Hastelloy-C276, after the purge of

the sampling line. At each time the sampling cell was previously filled with 6 to 12 mL of 1 M NH_4OH solution (*Suprapur, Merck*®) in order to dissolve the sampled (sour) gas in a basic solution. The sampling duration was short, on the order of a "fraction of" second, in order to avoid an oversampling by condensation of the gas at low temperature. The mass of ammoniac solution previously introduced in the cell and the mass of sampled fluid (0.5 to 2 g) were weighed. After one hour of reaction at room temperature the sampling cell was opened and the ammoniac solution is diluted in 2%HNO_3 solution (bi-distilled from *Suprapur, Merck*®) for further analyses by high-resolution mass spectrometry (HR-ICP-MS, *Element XR, ThermoScientific*®).

At the end of the experiment the reactor was decompressed and then flushed with argon before cooling to avoid the deposition of possible secondary phases during quenching. The temperature decreased below 300°C in 10 to 15min during this operation, and then the reactor was quenched at room temperature in air in one hour. This procedure prevents any back reaction during the quench. During decompression, the gas was analyzed for CO, H_2S and SO_2 by a *GasAlertMicro5* gas controller commercialized by *BW-Technologies*®. These measurements were restricted to dry gas because the condensation of water is incompatible with the electrochemical cell of the controller. We also sampled in one run an aliquot of gas in a Tedlar bag for analysis of the species OCS (predicted by thermodynamics) by micro-chromatography coupled with mass spectrometry (*MicroGC Agilent QUADH*). $SO_{3(g)}$, which is unlikely under these reduced conditions, was not analyzed.

The reacted samples were examined by several mineralogical techniques. The experimented material was systematically observed under SEM, as-is or on a polished cross-section. SEM observations were performed with *Geol-6360LV* microscope equipped with a *Brucker*® EDS, in both secondary electron imaging mode (SEI) and/or backscattered electron mode (BSE) on carbon-coated samples or polished cross-section sections. The analytical conditions for punctual chemical analysis were 20 kV, 10^6 counts and a working distance of 14 mm. The standards used for quantitative chemical analysis consisted of jadeite (Na), corundum (Al), wollastonite (Si, Ca), MgO (Mg), orthoclase (K) and metals for Fe, Mn and Ti. The matrix corrections were performed using integrated programs (PhiRhoZ correction).

Run	T (°C) ±3°C	duration (day)	$X(H_2O)$	initial density ($g.cm^{-3}$)	P (bar)	ΦH_2O (MPa)
V1	466	5	0	0.079	108-100	0
V3	470	6	0.50	0.135	218-115	8.44
V4	464	6	0.11	0.128	180-110	1.82
V6	456	5	0.75	0.157	253-215	12.5
V7	460	6	1	0.0534	150	12.8

***Table 2**: Experimental conditions for CO_2-H_2O systems. In each run, beads of picritic basalt, altered basalt and obsidian were reacted together. The gas was not sampled. X H_2O and Φ H_2O were calculated by processing the monitored P,T data through EOS models (Bakker, 2009).*

Run	T (°C) ±5°C	duration (day)	samples	*-------- mole loaded -------* "Venus" mixture	CO_2	H_2O	P (bar)	*------- calculated --------* XN_2	XH_2O	□ H_2O (MPa)	*------ measured ------* CO -----	H_2S ppmv (final) ----	SO_2	*calculated* log (fO_2)
V8	466	7	Obs, PB, 0.011g AB	0.345	0.452	0	169-136	0.03	0	0	0.05%	0†	0†	-24.3
V10	488*	3	Pum, 0.21g BG, Obs, PB	0.192	0.483	0	127-117	0.02	0	0	112	0†	0†	-21.3
V11	471	6	Pum, 0.17g BG, Obs, PB	0.177	0.435	0	98-94	0.02	0	0	176	48	688	-23.2
V13	473	14	8.0g YB	0.163	0.45	0	118-78	0.019	0	0	64	36	46	-23.5
V15	472	8	6.17g BG, BS	0.134	0.439	0	111-90	0.016	0	0	88	28	320	-22.5
V18	471	7	2.1g YB, 1.04g fBG	0.107	0.402	0	98-96	0.015	0	0	17	19	140	-21.5
V18bis	473	7	V18 continued	---- 2% CO added -----			85-82		0	0	-	-	-	-27.3
V12	470	2	Pum, 0.08g BG, Obs, PB	0.206	0.395	0.06	119-99	0.022	0.13	1.28	-	-	-	
V14	471	16	7.3g YB	0.165	0.211	0.22	102-87	0.019	0.38	3.16	-	-	-	
V19	471	7	Pum, Obs, BG	0.113	0	0.36	90-87	0.017	0.78	5.57	-	-	-	
V17	468	9	Pum, 2.0g BG, Obs	0.123	0.29	0.36	138-127	0.011	0.49	6.03	-	-	-	
V22	472	30	Pum, Obs, BG, PB	0.099	0	0.406	90	0.014	0.82	6.67	-	-	-	
V21	470	1.5	Pum, Obs, BG	0.096	0	0.424	90-85	0.013	0.83	6.92	-	-	-	
V20	472	7	Pum, Obs, BG	0.142	0	3.18	360-355	0.003	0.96	23.0	-	-	-	
V23	473	7	Pum, Obs, BG, PB	0.229	0	4.95	590	0.003	0.86	29.5	-	-	-	

***Table 3**: Experimental conditions for the Venus-like systems. PB= picritic basalt, Obs= obsidian, AB= altered basalt, Pum= basaltic pumice, BG= basalt glass, YB= crystallized basalt, BS= basalt slide, fBG= grinded basalt glass. When mass is not indicated means sample as bead. * V10 underwent two accidental cooling during the run, down to 178°C and then down to 25°C. † V8 and V10 were not sulfurized sufficiently to exceed the reaction with the vessel walls. X H_2O and □ H_2O were calculated by processing the monitored P,T data through EOS models (Bakker, 2009). fO_2 was calculated from the CO/CO_2 ratio and Eq.(27) in Fegley et al. (1997). The pressure range corresponds to the decrease of pressure by leakage.*

When secondary products were identified in significant amounts, they were recovered by sonification/decantation in alcohol and characterized by XRD on oriented preparation (decantation on glass slides and analyzed as-is or after glycolation). XRD analyses were performed on a *Bruker® D8* XRD diffractometer ($CuK\alpha^{1+2}$ radiation) over the 2-60° 2Θ angular range with 0.02° 2Θ steps and 2 seconds per step.

The altered surface of the polished basalt glass slide was analyzed by XPS and HR-TEM. XPS analyses were performed on a *ThermoScientific®* spectrometer (Kalpha) using a monochromatized Al Kα (1486.6 eV) source. The Pass energy was fixed at 40 eV with a step of 0.1 eV for core levels. Ionic Sputtering of the surfaces was made by Ar^+ ion beam accelerated under 1 keV. XPS Spectra were recorded in direct N(Ec). The analyzed surface area is 400 µm in diameter and less than 10 nm in depth. The photoelectrons spectra are calibrated with respect to the C1s at 285.0 eV (+/- 0.1eV) energy. The HR-TEM analyses were performed on ultrathin sections using a *JEOL JEM-ARM200F Cold FEG* microscope coupled to *CENTURIO-X*, an energy-dispersive X-ray spectrometer and an electron energy loss spectrometer. The sample has been prepared by using focused ion beam (FIB) technique using electronic microscope *HELIOS 600i (FEI)*.

3. Results

3.1 Redox conditions

Redox conditions of the Venus-like experiments were assessed from the carbon speciation as measured at the end of the dry-gas runs. Oxygen fugacity was calculated from the CO/CO_2 concentration ratio and Eq. (27) reported in Fegley *et al.* (1997). The values are reported in Table 3 and fall in the 10^{-21}-10^{-27} range, with an average value at $10^{-23.4}$ consistent with the Ni-NiO mineral buffer at 470°C. This is consistent with the composition of the reactor, a Ni-based alloy. This redox range is significantly below the hematite-magnetite buffer and over the magnetite-wustite buffer meaning that the most stable form of iron oxide is magnetite, in agreement with that which is generally admitted for the Venus surface, at least at low elevation (Fegley *et al.*, 1997).

The sulfur chemistry is more complex with several species of intermediate degree of oxidation and several possible redox reactions involving S° and H_2O. For example, the reaction $SO_2 + 3H_2 = H_2S + 2H_2O$ has to be considered. But in absence of accurate measurements of elemental sulfur and molecular water in the "dry" gas, the sole concentrations of H_2S and SO_2 are not sufficient to determine the redox state of the sulfur system and to check if the sulfur speciation is in redox equilibrium with the carbon speciation. However, the concentration of OCS measured in run V11 indicated a value of 18ppmv, in the order of magnitude of the current composition of the Venus lower atmosphere (Marcq *et al.*, 2008). In addition, basic thermodynamic calculations show that possible H-species like H_2 or CH_4 are unlikely in our relatively oxidizing conditions.

Although our experiments are not designed for an accurate determination of sulfur speciation, we believe that the gas composition in our Venus-like experiments is likely not so far from present-day Venus deep atmosphere.

3.2 Reaction products

A constant observation in all of the runs is the deposition of fine metal-rich particles on the samples. The composition of these particles depends on the run conditions: Ni, Mn, Mo oxides in pure CO_2 or metallic sulfides in Venus-like atmosphere. These particles may be related to a metal dusting-like process, a corrosive disintegration of alloys into fine particles in carbon-saturated atmosphere occurring typically between 400 and 800°C (Agüro *et al.*, 2011, a review).

Another constant observation is the higher reactivity of olivine and glasses over plagioclase and pyroxene, as it is frequently the case in aqueous silicate alteration. There is only one exception (discussed at the end of the paper) where olivine appeared inert, under 590bar H_2O. Consequently, we mainly focus here to the behavior of olivine and glasses. We also distinguish the observed reactions in the simplified CO_2-H_2O system from those in the Venus-like system.

3.2.1 Pure CO_2-H_2O system

The first run conducted in dry CO_2 did not show any sign of alteration when observed under SEM. By contrast, the increase of H_2O content in the gas led to progressive morphological changes of olivine and obsidian surfaces (Figure 1). For olivine, the surface shows signs of recrystallization that depends on H_2O:CO_2 ratio. At lowest tested ratio ($X$$H_2O$ = 0.11) some exposed faces seem unmodified while others exhibit a very thin altered film. At the highest H_2O:CO_2 ratio, or in pure water, three morphologies of crystals were observed: fibrous, lamellar or massive crystals. The volume of newly formed crystals did not allow a chemical or crystallographic characterization by SEM or XRD methods. For obsidian, the alteration is more pronounced and alteration layers are thick enough to be observed on polished cross-section. In Figure 2 we show the SEM observations of altered obsidian at $X$$H_2O$ = 0.50 and 0.75. Polished cross-sections reveal under SEM the development of crystallized silicates within a surface layer of several tens of micrometers. For $X$$H_2O$ = 0.75, quantitative EDS analyses evidence a mixture of few iron oxides, anorthoclase (>90%) and a Fe-bearing amphibole of the hornblende group. To improve the mineral determination of the alteration layer we carried out *in-situ* XRD on the polished section for several days. Despite this long accumulation time, the diffractograms were poor in reflections with a pronounced baseline. This may be due to the small surface area exposed to the X-ray beam (0.1cm^2), a possible preferential crystal orientation and likely a low crystallinity of the material. In addition, we masked undesired zones of the section by a Pb-film so some intervals of the pattern have been removed corresponding to Pb and its oxides. The two diffraction patterns showed in Fig. 2 are accumulations of several diffractograms and show two kinds of pattern: weak reflections consistent with hornblende and two small diffuse bands at the position of

the main plagioclase pattern (anorthoclase from SEM). The low intensity of anorthoclase pattern, while it is the dominant constituent of the altered layer, indicates a low degree of crystallinity or more likely a small crystallite size, probably less than 50-100nm. The low number of lines, when compared to a powder reference spectrum, may be attributed to a preferential orientation of the crystallites. At $XH_2O = 0.50$ the alteration layer is not well organized and it is depleted in silica and enriched in alkali. At the lower H_2O content ($XH_2O = 0.11$) we did not observe any alteration layer suggesting that a threshold concentration may be necessary for glass crystallization.

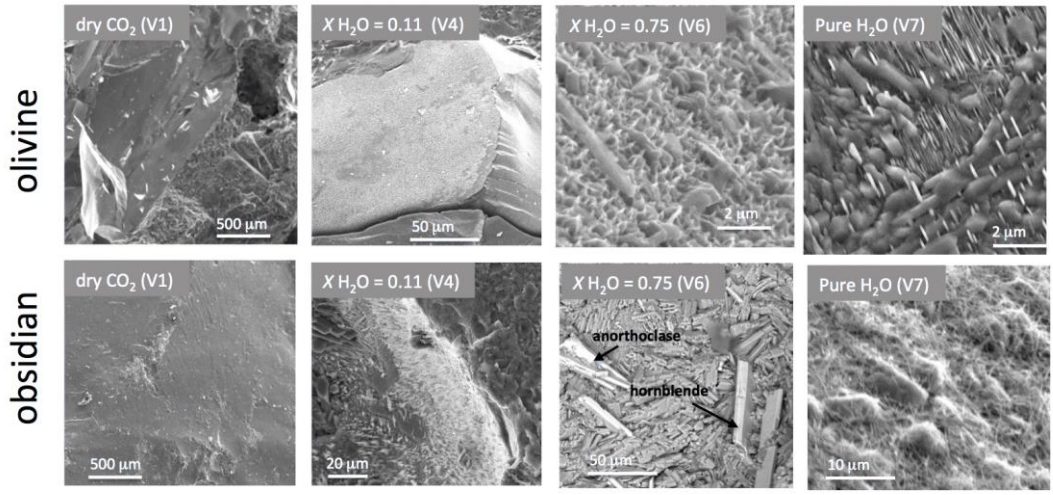

***Figure 1**: Morphology under SEM of altered olivine and obsidian glass in the pure CO_2-H_2O system.*

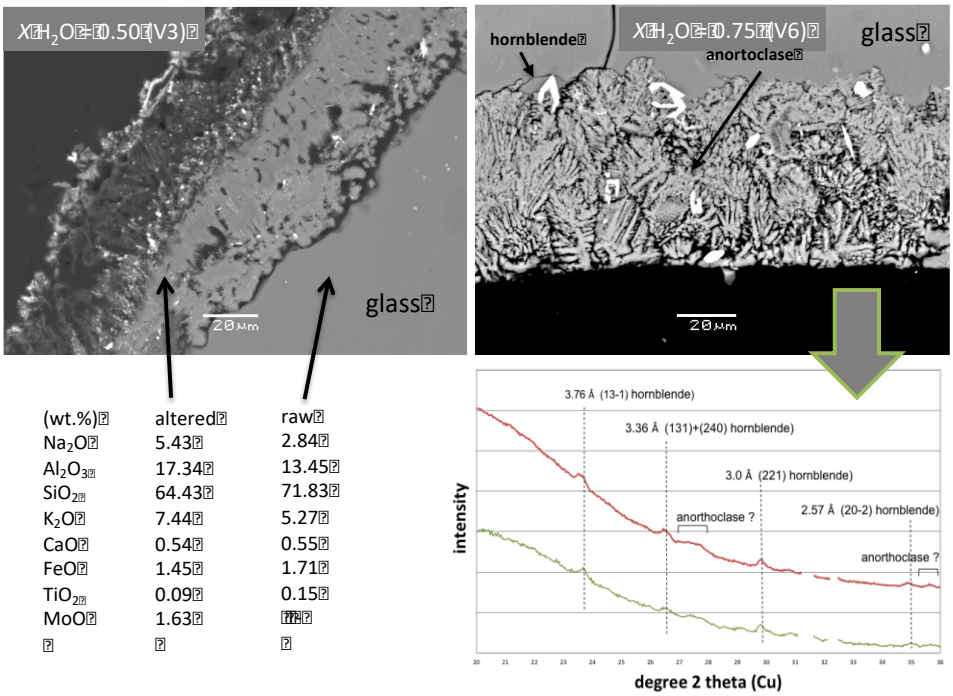

***Figure 2**: SEM observations of a polished cross-section of altered obsidian and basalt glass in H_2O-CO_2 system, and the associated XRD pattern.*

The clay fraction (corrensite) of the reacted altered basalts conserved its crystallinity and its swelling properties in wet gas (Figure 3). When reacted in dry CO_2, the collapse of the pattern reflects a loss of crystallinity but the 2:1:1 structure, evidenced by a band at 14Å, is conserved. By contrast, when heated in air at 470°C for one week the 2:1:1 structure is lost and the pattern is flat.

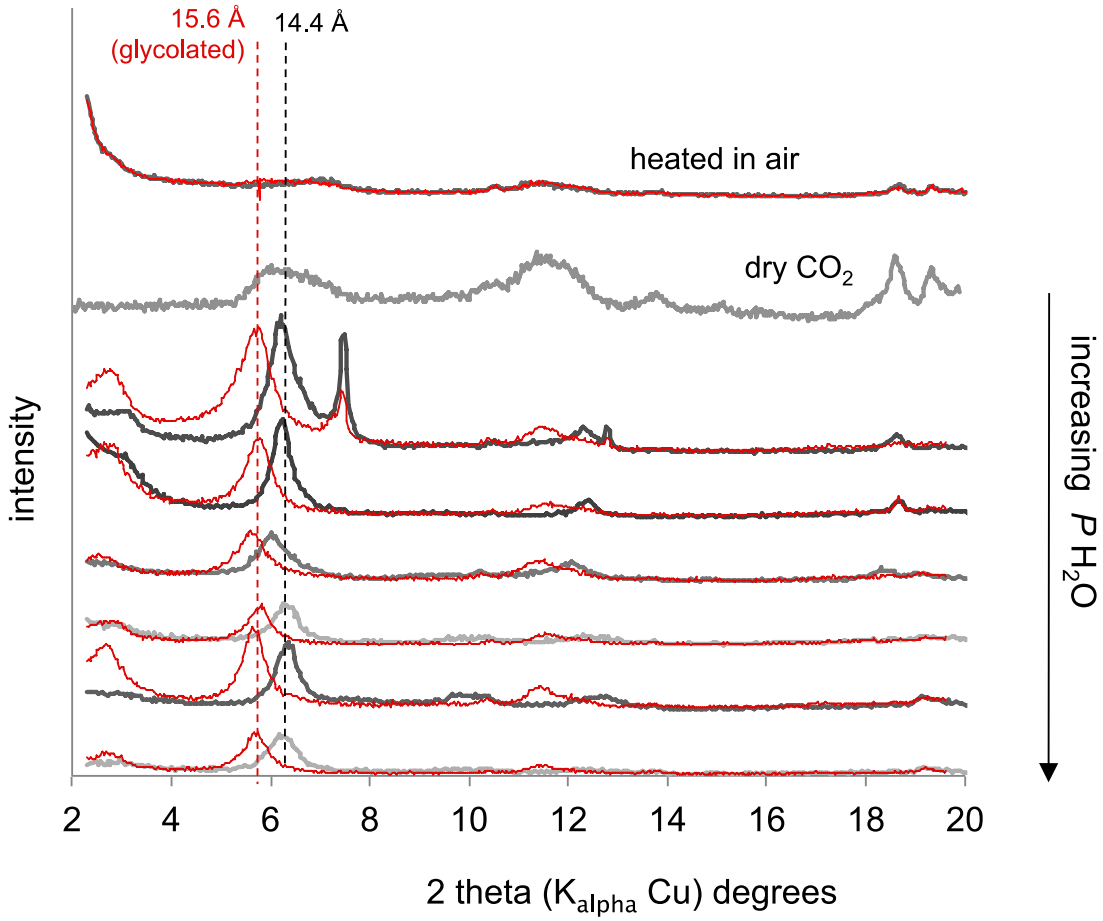

***Figure 3**: XRD patterns of the oriented clay fraction from the altered basalt exposed to increasing H_2O content in the H_2O-CO_2 system. The red curves are for glycol-saturated preparations.*

3.2.2 Venus-like system

In this suite of experiments we tested the consequence of adding sulfur-bearing species on the above process. We also tested different materials. In particular, we reacted a natural basaltic pumice, a crystallized basalt and the basalt glass as powder, in addition to the previous tested materials. The main observation is the formation of sulfur-bearing species at the surface of the samples, mainly the glassy materials. Some examples are shown on Fig. 4.

In dry gas, surface of glasses was covered by S-bearing crystals of several microns in size, likely sulfates. In the run using glass beads with XH_2O=0.36 (V17) we were able to recover the secondary

minerals by sonication in alcohol and their XRD pattern indicated the presence of anhydrite, confirming that these salts are sulfates. In a given run, the sulfate composition seems to be dependent on the nature of the support: anhydrite on basaltic glass and obsidian, anhydrite + (meta)thenardite (Na_2SO_4) + glauberite ($Na_2Ca(SO_4)_2$) on pumice, for example. This suggests a local source of cations for the sulfate nucleation and growth. However, this can differ from one run to another: Na_2SO_4 rather than $CaSO_4$ recovered the basaltic glass slide in V15. By contrast to glass, olivine in dry gas does not produce detectable sulfate but rather an iron oxide coating (V11). It is also interesting to note that iron sulfide, likely pyrite, forms on the picritic basalt during an accidental cooling (V10). We did not observe sulfide in the other runs. This is consistent with thermodynamic findings of the pyrite-magnetite buffer predicting the stability of pyrite at high elevations, i.e. low temperature (Fegley *et al.*, 1997).

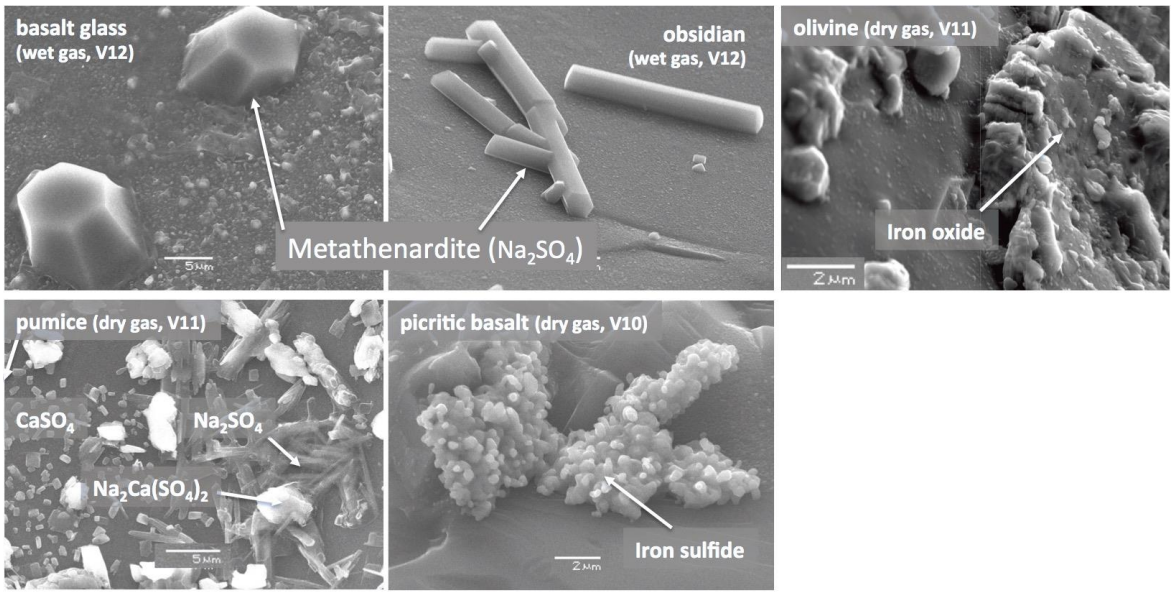

***Figure 4**: Examples of sulfurized species that grew on the surface of samples altered in Venus-like gas.*

In wet sulfurized gas, (meta)thenardite, sometimes enriched in Fe, dominates over the other sulfates. Olivine of the crystallized basalt reacted in wet sulfurized gas (V14) exhibits fibrous material at the surface that we were not able to identify. By contrast, the glass beads tested in run V17 produced enough secondary phases to be isolated by sonication/decantation in methanol and characterized by XRD. Beside anhydrite we clearly identify a non-swelling clay mineral of the chlorite group and a 10Å phylosilicate mineral, likely celadonite. This last one, a common alteration phase of basalts, is also detectable in the bulk reacted fraction suggesting that it is not limited to the surface.

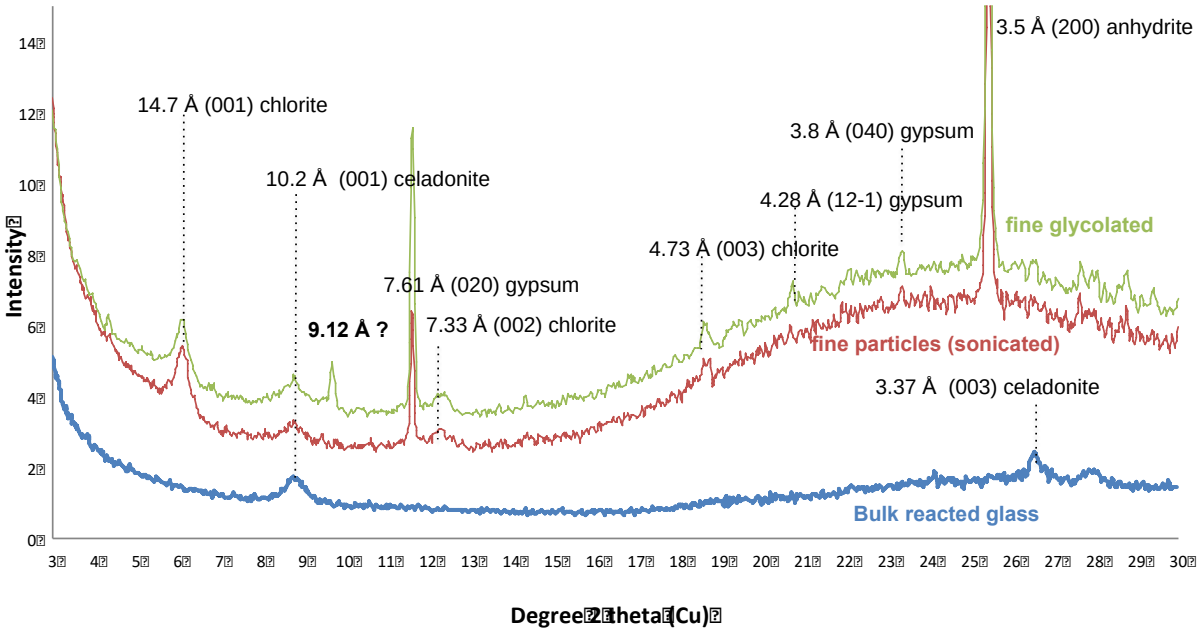

***Figure 5**: XRD patterns of the alteration phases produced on basalt glass in wet Venus-like gas (V17)*

In order to better understand the formation of sulfate crystals on the glassy surface in dry gas, the basaltic slide was analyzed by XPS. This surface sensitive analytical method provides the chemical composition of a centimeter surface area for a thickness that does not exceed few nanometers. Variation of composition with depth is measured after successive sputtering of the surface with an argon ion gun. We carried out analyses on three reacted slides. The first reacted slide was dedicated to a depth profile through the sulfate layer (approximately 1 micron) by a progressive sputtering with the ion gun and a total etch time of 1500 sec. The two other altered slides were pickled before the XPS analysis, either mechanically with a cutter blade or chemically by a brief water rinse in order to better assess the glass composition below the sulfate layer. The following elements (electron energy level) were quantified: Al(2p), Si(2p), S(2p), K(2p), Ca($2p_{3/2}$), O(1s), Fe($2p_{3/2}$), Na(1s) and Mg(1s). The sulfur concentration decreased through the sulfate layer from 10 to 4 %atm, from 7 to 0.9 %atm in the scraped sample and from 0.6 to 0 %atm in the washed sample. This succession of the three samples mimics a wide depth profile from the sulfate-rich surface to the interior of the glass. Unfortunately there is no obvious equivalence between the etch time and a quantified thickness. However, it is likely that we did not probe deeper than 100 nm inside the glass. The results are presented in Figure 6 after the following data processing. The concentrations in atom % are normalized to 100 after removing the contribution of S and its associated O and Na based on the thenardite stoichiometry. This approach provides focus on the glass composition itself. In a second step, the concentrations are normalized to the composition of the pristine glass (Table 1) in order to quantify the gain or loss of each element as a function of the etch time (depth). The first analyses before the 50 sec etch time are ignored to discard

any surface contamination, typically C and O. The results show a strong accumulation of Na at the surface, a gain of Mg and a loss of Ca beneath the interface with the sulfate layer. Fe shows a deficit in the sulfate layer, less pronounced but possible in the interior of the glass. Si and K do not show significant variations, at least in the accuracy of the XPS quantification (20-30% relative).

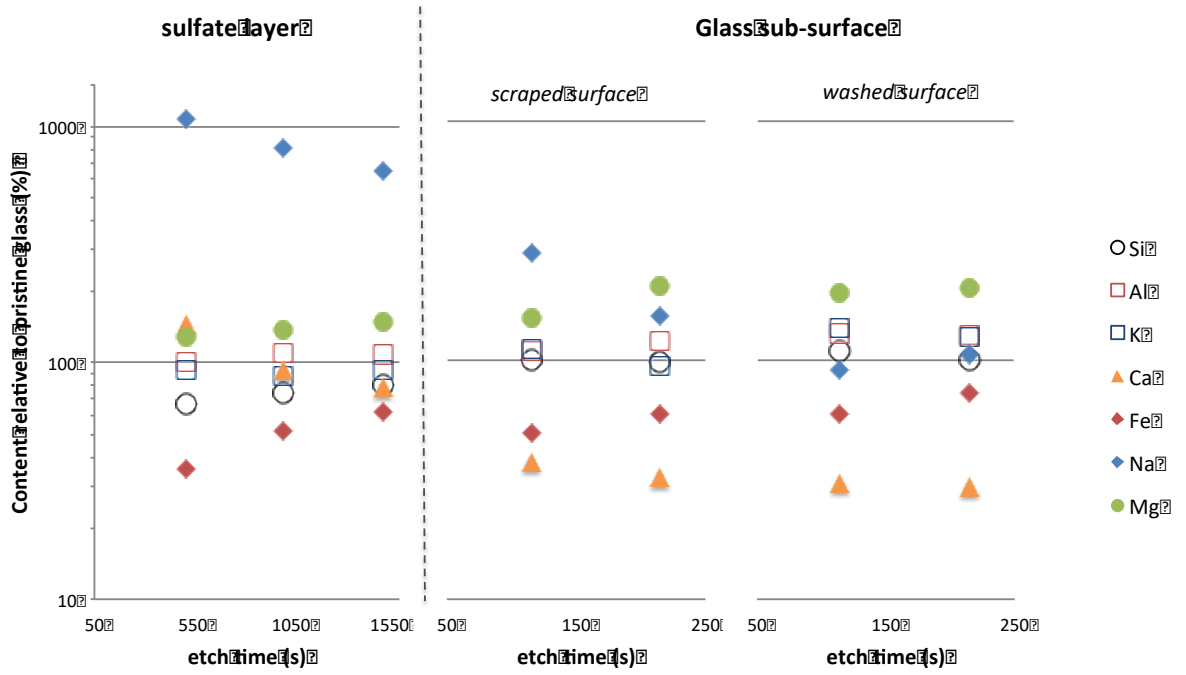

***Figure 6**: Relative chemical gain and loss at the sub-surface of the basaltic slide altered in the dry Venus-like gas (V15), as measured by XPS. The stronger variations are the accumulation of Na in the sulfate layer and the loss of Ca deeper in the glass. A general gain of Mg and loss of Fe is also observed.*

The XPS analyses were complemented by HR-TEM microanalyses. An ultrathin section of the altered glass slide (V15) with the precipitated $(Ca,Na_2)SO_4$ salt coating was been prepared by the FIB technique. The HR-TEM/EDS analysis showed the distribution of principal major elements in the alkaline basaltic glass at the interface with the salt coating (Figure 7). Below the interface with the salt coating, we observed dendrites in the glass matrix of the sample. The dendrites are enriched in Fe, Mg and Ti crystals (Table 4, point a). The crystal diffraction images and the characteristic d (Angstrom) and d-spacing indicate the dendrite mineral has a spinel structure, magnesioferrite ($MgFe_2^{3+}O_4$). The investigated glass around the dendritic zone is depleted in Fe, Mg and Ti, as well as in Ca and Na compared to the starting glass composition (Table 4 points b and c). Moreover, the investigated glass around the dendritic zone is enriched in Si and Al compared to the initial composition of the glassy sample (Fig. 7).

Phase Point position/ Atom%	Dendrite a	Glass b	Glass c	Pristine glass
O	54.0	58.1	54.9	52.5
Na	0.7	0.2	1.8	2.4
Mg	10.8	6.1	8.2	11.9
Al	3.8	5.9	5.1	3.8
Si	11.8	24.3	20.4	16.6
K	0.4	0.5	0.5	0.2
Ca	1.8	2.2	4.8	8.2
Ti	1.0	0.2	0.5	0.8
Fe	15.7	2.6	3.4	3.8
Total	100.0	100.1	96.6	100.2

Table 4: *HR-TEM/EDS standardless quantitative analysis of the alkaline basaltic glass slide (V15)*

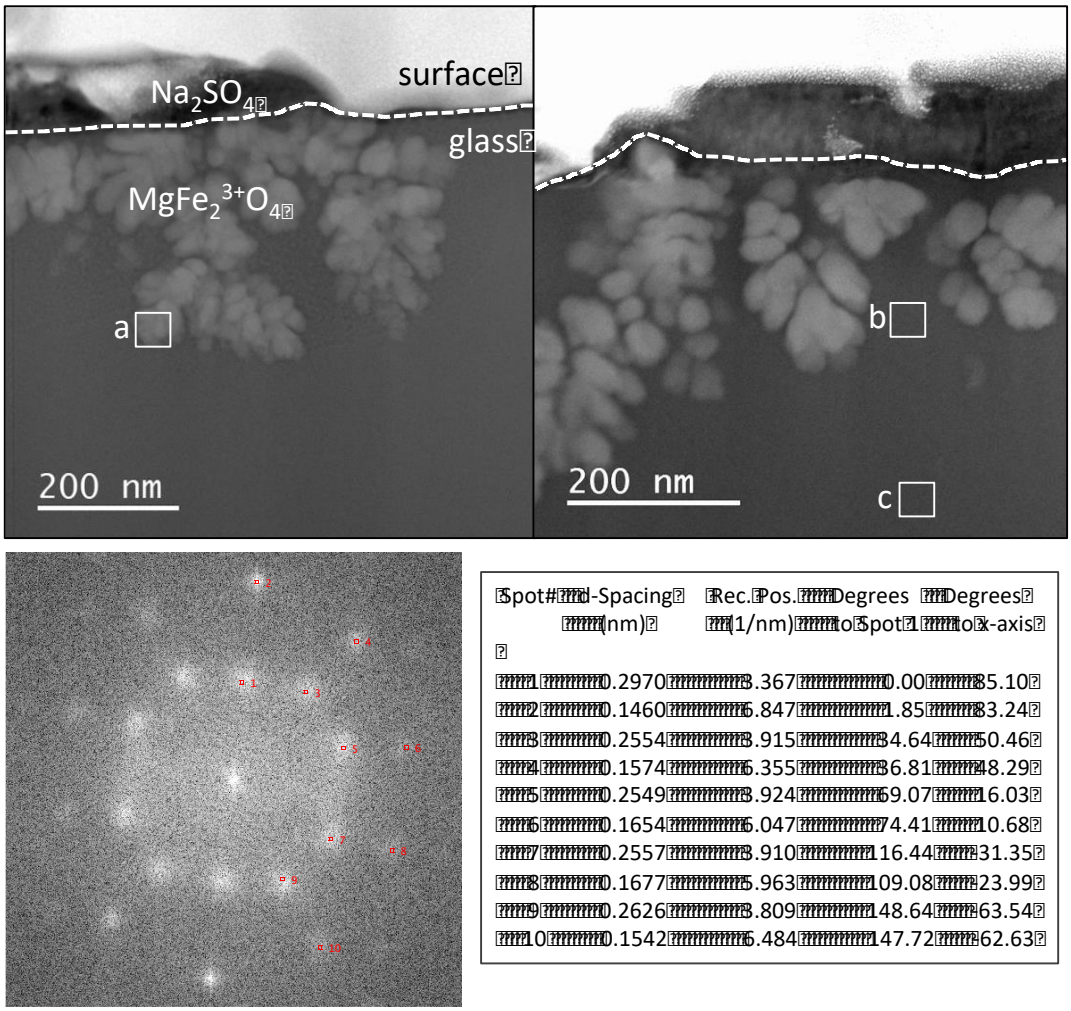

Figure 7*: Bright field transmission electron micrograph of an ultrathin section of the altered glass slide surface (V15, dry gas). Salt, $(Ca,Na_2)SO_4$, is visible in the upper part of the sample and dendrites in the glass below the surface. The location of the analyzed zone by EDS is indicated by squares. An example of a diffraction image with d-spacing is reported in the lower cases*

3.2.3 High water pressure test

In order to better assess the role of vapor pressure, a few runs were conducted under up to 590 bars of H_2O-rich gas, well above the usual range. These runs lasted one week and focused on glassy materials. Pumice, synthetic basalt glass and obsidian altered through different pathways: pumice and basalt glasses developed a chemically modified layer, depleted in Ca for basalt glass or hydrated for pumice, without true recrystallization (Fig.8a). For the higher tested vapor pressure, the core of the obsidian grain, beneath the recrystallized rim, was slightly modified (Fig.8b): its color turned from black to green and it appeared porous (black infra-micrometric holes in Fig.8c) or hydrated. The chemical composition of the core was not significantly modified, while the recrystallized rim is depleted in silica. Figure 8 shows the most spectacular observations on polished cross-section under optical microscope and SEM. In all the cases, sulfate minerals were observed at the surface of the altered samples.

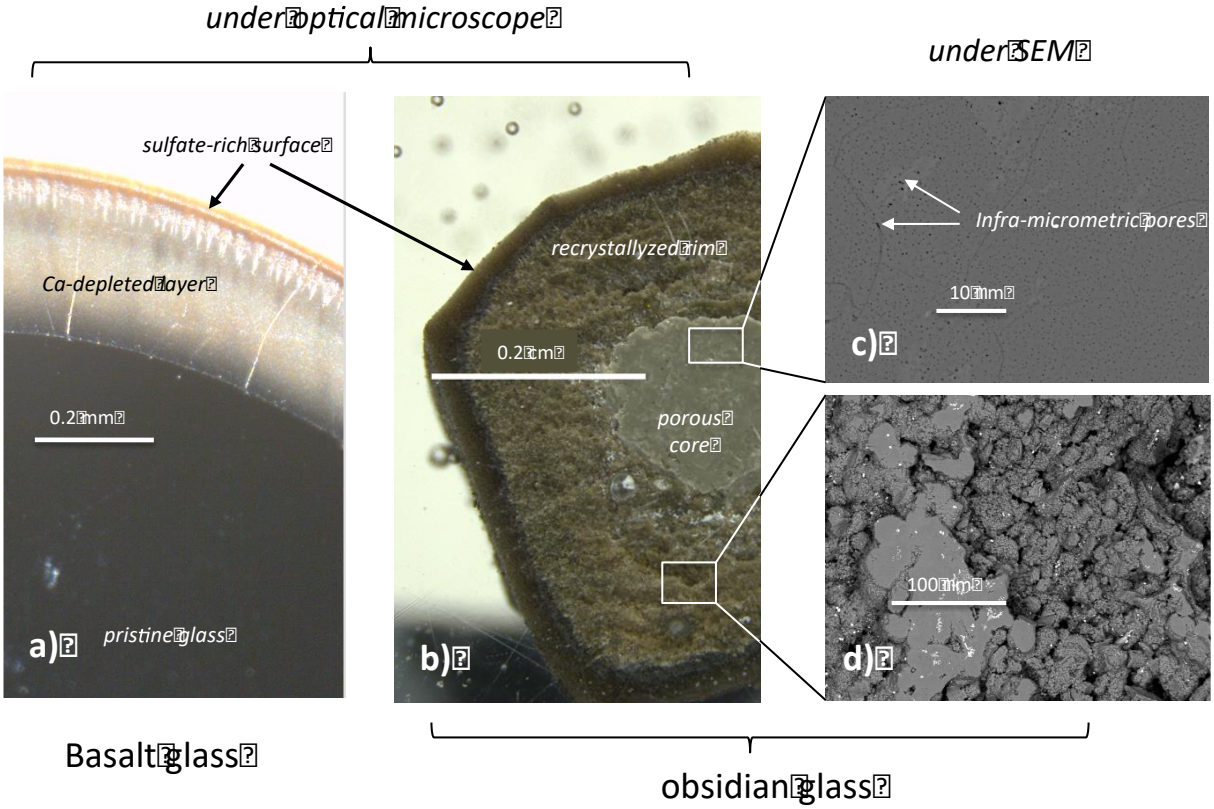

***Figure 8**: Crossed section of altered obsidian and basalt glass (for comparison) observed under optical microscope and SEM. Samples were altered one week under 590 bars vapor-rich pressure (V23). a): basalt glass with a sharp leached surface layer. b): Obsidian with a recrystallized rim and a modified core. c): small pores (black holes) in the modified obsidian core. d): details under SEM of the recrystallized rim.*

The reaction rates are reflected in the thickness of the alteration layer developed as a function of time. Fig. 9a reports the dependence of the recrystallized rim thickness on elapsed time for a constant water fugacity of 6-7 bars. The first-level observation shows that reaction rates also depend on the water pressure all of the other parameters being constant. In order to quantify the role of water pressure on alteration kinetics, we compare in Fig. 9b the thickness of the recrystallized rim after one week of reaction to the water fugacity that varied over one order of magnitude in six selected runs. We choose obsidian as a reference material because it reacted fast enough at laboratory time scale to make measurements easily even at low vapor pressure. In this figure we also reported a predicted alteration thickness extrapolated from the rate constants reported in the literature for condensate water below 300°C. The "long term" rate constant in Si-rich solution reported in Berger *et al.* (1994) was extrapolated to 470°C. It corresponds to the steady state dissolution rate when the solution is enriched in silica by the glass dissolution. Considering that this situation is comparable to the rate observed here after one week of reaction, we first calculated the rate constant measured at 470°C from the data measured at lower temperature and assuming an activation energy of 60kJ.mol^{-1}. The extrapolated value ($7x10^{-5}$ mole Si.m^{-2}.s^{-1}) was then converted in altered thickness for 7 days of reaction using a glass density of 3 kg.dm^{3} and a Si concentration of 0.025 mol.cm^{-3}. We found a recrystallized thickness of 1.7 mm assuming that the dissolution rate of the pristine glass controls the progression of the recrystallized rim. This value is reported in Fig.9b assuming that the density of a liquid aqueous system heated at 470°C decreases down to 0.3 and the pressure increases to 60MPa, the corresponding water fugacity being 31Mpa. It is worth noting that the value extrapolated from lower temperature in Fig. 9b is consistent with our measurement at high fH_2O suggesting an equivalent rate at water equivalent density. However, the assumption of an unchanged activation energy above the critical temperature is not expected as mentioned in the introduction and the predicted value (blue star) is perhaps overestimated. In addition, the basalt glass reacts much more slowly than obsidian. The uncertainties are not reported in the figure: they can reach 25% for the experimental observations (high fluctuation along the surface) and for the predicted value (blue star) it is dependent on the assumption used for the water density and basalt dissolution rate constant. So this conclusion is an interesting kinetic insight but should be taken with caution. It is also worth noting the rate dependence on water fugacity takes a non-expected form with a strong increase of the rates under high pressure. By contrast, the rate dependence with time suggests an expected control by diffusion (linear relationship with $t^{1/2}$), likely diffusion of water through the recrystallized layer.

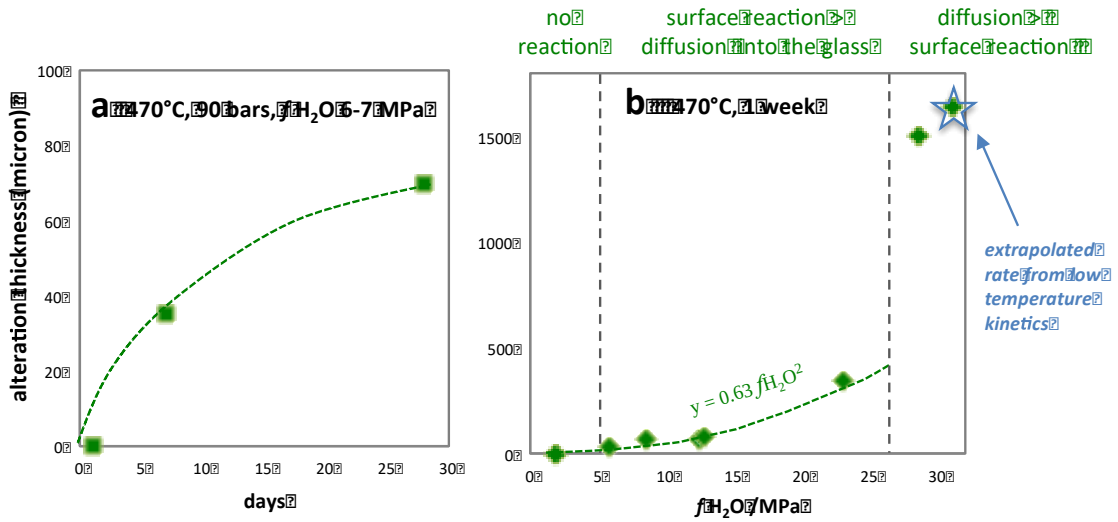

***Figure 9**: Dependence of the recrystallized rim thickness of obsidian glass on water fugacity (a) and on elapsed time for fH_2O= 6-7 bars (b). Refer to the discussion for the meaning of the dashed lines*

3.3 Gas chemistry

The concentrations of the usual samples components in the sampling ammonia solutions are significantly higher than the ICP-MS detection limit, the blank of chemicals or the contamination of the sampling cell. They reflect undoubtedly the gas composition inside the reactor. They were converted into gas concentrations using the ammonia/sampled gas mass ratio. The data is chronologically reported in Figure 10 as it was measured run after run. The figure also includes blank experiments (run without sample) carried out before V15 and V18 (see Table 3). Before V13 the sampling method was not optimized (use of NaOH instead of NH_4OH), the results are thus less reliable and are not reported in the figure. Whatever the samples tested (glassy, crystallized, blank) the measured concentrations decreased with time, sampling after sampling, suggesting that we measured a decreasing contamination. An outstanding exception is the run using a fine powder of basalt glass (V18), with a higher sample surface area than the remaining runs. In this run, the three fluid samples were significantly enriched in Na, Mg and Ca, the same elements forming secondary sulfates and showing content variations at the glass slide surface. However, these unusual high concentrations dropped in the successive repeated sampling suggesting that we more likely measured an accumulation of these elements in the sampling line rather than a true concentration in the gas. We did not measured a Fe enrichment even though this element is detected in some secondary sulfates (and hornblende) and showed a concentration loss to the glass surface.

The high concentration of Na in the first reported runs (V13) likely reflects a contamination due to the use of NaOH is the sampling method before V13. This shows how difficult the decontamination of

the reactor and sampling device may be. Another example is silica, the initial contamination of which being likely related of previous experiments conducted in this reactor.

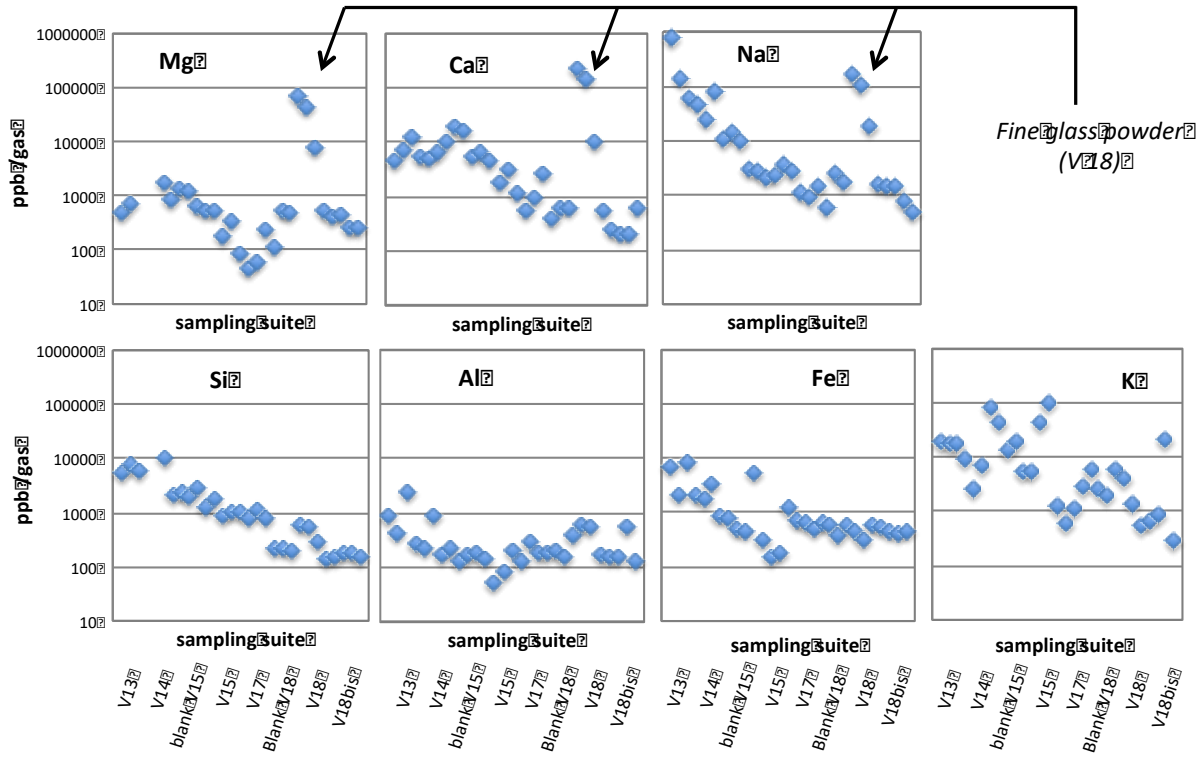

***Figure 10**: Major components of the samples measured in the gas sampling after sampling.*

4. Discussion

4.1 Transfer in gas

The concentrations of the rock constituents measured in the gas phase (roughly 0.1 to 100 ppm) decreased run after run. This decrease does not seem related to the samples exposed to alteration (blank experiments do not distinguish from experiments with rock samples) or the conditions of alteration (dry or wet gas), excepted run V18 where we measured a significant increase of Mg, Ca and Na concentration in the gas related to the high surface area of the sample. For the other runs, the regular decrease of gas concentration with time rather suggests a contamination from the reactor that decreases with time. Our results nevertheless show that a significant mass transfer occurred. Firstly, the contamination is a mass transfer itself. The measured concentrations (> 1ppm Fe, Ca and Na; 0.1ppm Al and Mg) are also much higher than the sulfates or oxides solubilities in gas as expected from thermodynamic databases (not developed in this paper) with the exception of silica. For silica, the measured concentrations decreased down to values in the order of magnitude of $Si(OH)_4$ in H_2O-CO_2 gas mixture equilibrated with solid silicon oxide (Plyasunov, 2011). We indeed observed the formation of silica spherules in the colder part of the magnetic driver in preliminary runs (Berger and

Aïgouy, 2011). These lepidospheres are common in volcanic gas and can even be observed in the vacuoles of the obsidian sample used in this study. They could be the source of Si contamination. However, we did not observe lower values in dry gas suggesting than the gas composition in our experiments is likely not controlled by equilibrium thermodynamics, or at least not by the solubility products of usual mineral or gas species.

Another evidence of gas transfer is the observation of chemical changes in the reacted samples. The behavior of iron is a typical example. The formation of iron oxide coating at the surface of olivine in dry gas indicates diffusion of Fe to the olivine surface. This coating may result from iron accumulation on the surface after release of Si and Mg into the gas (we also observed a loss of silica in the altered obsidian glass at low H_2O:CO_2 ratio, Fig. 2). Alternatively, the Fe-coating at the olivine surface may also have a contribution from the gas, as well as the crystallization of Fe-hornblende at the surface of reacted obsidian or the formation of iron sulfide during an accidental cooling (V10).

Another evidence of elemental mobility concerns Mg, Ca and Na. These elements showed evidence of migration in the basalt glass at nanometric scale (Fig. 6), likely correlated with the high concentration measured when using glass sample with high surface area. The analysis of the results suggests that these elements were likely deposited in the colder part of the sampled line (after a gas transfer) and were leached during the successive sampling.

The factor promoting the elemental transfer in the gas phase is an open question. The absence of positive effect of CO-enriched gas (run V18bis) discards the assumption of carbonyl complexes as vector of transfer as suggested in Simakin *et al.* (2016). The most likely explanation for the observed transfers is that they are controlled by thermal gradients, with deposition in the colder zones. Even at low concentration, the diffusion and the precipitation kinetics at high temperature are high enough for a significant transfer at the time scale of the week and the space scale of tens of cm.

4.2 Process in dry gas

Alteration in the absence of water might be unlikely given the low dielectric constant of CO_2. However, the presence of dipolar molecules such as SO_2 or H_2S may promote the silicate network depolymerisation. Furthermore, some alteration phases are present in the basalt samples. Similar to King *et al.* (2018), we observed an iron oxide coating on olivine surface, although they detected Mg-sulfate as well. For the glasses in our experiments, the deposition of sulfate minerals and Fe-oxide is observed, like Renggli and King (2018). Our HR-TEM and XPS observations are consistent with oxidation experiments conducted at high temperature in the 90's. Cook and Cooper (1990) showed from Rutherford backscattering spectroscopy (RBS) and HR-TEM that oxidation of iron in a basaltic glass is accompanied by the migration of Ca, Mg and Na and crystalline nucleation of magnesioferrite. Cooper *et al.* (1996) proposed that CaO and MgO may precipitate at the surface of oxidized glass. Our XPS and HR-TEM observations are fully consistent with the chemical process proposed by these

studies with the difference that sulfates, rather oxides, form at the surface. The precipitation of $CaSO_4$, $MgSO_4$ and Na_2SO_4 by reaction of glasses with SO_2 gas has been recognized (see reviews by Palm *et al.*, 2018; Renggli and King (2018); Delmelle *et al.*, 2018). The experimental studies used 1 bar SO_2 and a temperature range above the present study. However, the same processes seem to govern the glass alteration, such as the composition of sulfate salts. The variability of sulfate composition (glauberite, anhydrite, metathenardite) observed here from one sample to another may be explained by the iron content and Fe^{2+}/Fe^{3+} ratio in the source material. As pointed by Renggli and King (2018), iron oxidation leads to Fe^{3+} transfer into tetrahedral coordination with Na^+ migration away from the surface (charge compensation), impeding Na_2SO_4 formation.

The above processes require redox reactions, at least for iron and sulfur. The redox conditions imposed by Ni/NiO buffer are consistent with oxidation of ferric iron although the fO_2 is too low in our experiment to reflect a direct reaction with di-oxygen as electron acceptor. Sulfur is present in the gas phase as sulfur dioxide SO_2 and in the solid phases as sulfate SO_4^{--}. The conversion of Ca,Mg-silicate to enstatite + quartz as suggested by Eq. 6 in Gilmore *et al.* (2017) cannot be the cause of SO_2 oxidation, the reported equations being not equilibrated in oxygen. The disproportionation of SO_2 into SO_4^{--} (sulfate) and S_x (polysulfur) is invoked in SO_2-basalt reactions (Zolotov, 2018; Renggli and King, 2018; Palm *et al.*, 2018). The conversion of CO_2 into CO + ½ O_2 is also a likely candidate for electron transfer and is thermodynamically favorable (Zolotov, 2018). Unfortunately we were not able to check whether SO_2/S_x or CO_2/CO couple controlled the sulfate formation in our experiments. However, Aveline *et al.* (2011) reacted basalt glass with pure SO_2 at 4.4 bar and 460°C for 3 years. They did not observe the formation of sulfate suggesting that glass oxidation and the concomitant elemental migrations require another electron acceptor than the sulfur disproportionation. CO_2 seems to play a role in these reactions. By contrast, Renggli and King (2018) experimented a variety of minerals and glasses in pure SO_2 gas under low pressure and temperatures above 600°C and observed the formation of sulfate in a CO_2 free system. Temperature may be critical for the redox reactions which control the bulk process. In our case, which is close to the temperature conditions of Renggli and King (2018), the reduction of CO_2 to CO may be the required electron acceptor reaction. Similarly, in the CO-enriched run (V18bis) iron sulfide is observed rather than oxide or sulfate in response to the more reducing conditions of this run. This is another indication of the role of carbon in these systems. However, the assumption of CO_2 reduction into CO at the glass surface as electron acceptor for sulfur dioxide oxidation (as well as iron oxidation within the glass) implies that the sulfur system was not initially in equilibrium with the carbon system. Whatever the explanation, electron transfer is the key process for glass alteration in dry gas. A synthetic view of the chemical reaction occurring at the glass surface is presented in Figure 11. For glasses in dry gas the reported transfers in the glass are similar to Figure 9 in Renggli and King (2018). For olivine, the formation of a residual iron oxide coating supposes the release of silica susceptible to react with the Mg-component of olivine to form enstatite as modeled by Zolotov *et al.* (1986,1991). As King *et al.* (2018) in similar

investigations, we did not observed enstatite suggesting that the excess of silica was rather released into the gas phase (or sequestrated at depth in the crystal) and was not consequently available for a local reaction, or it could be a matter of kinetics.

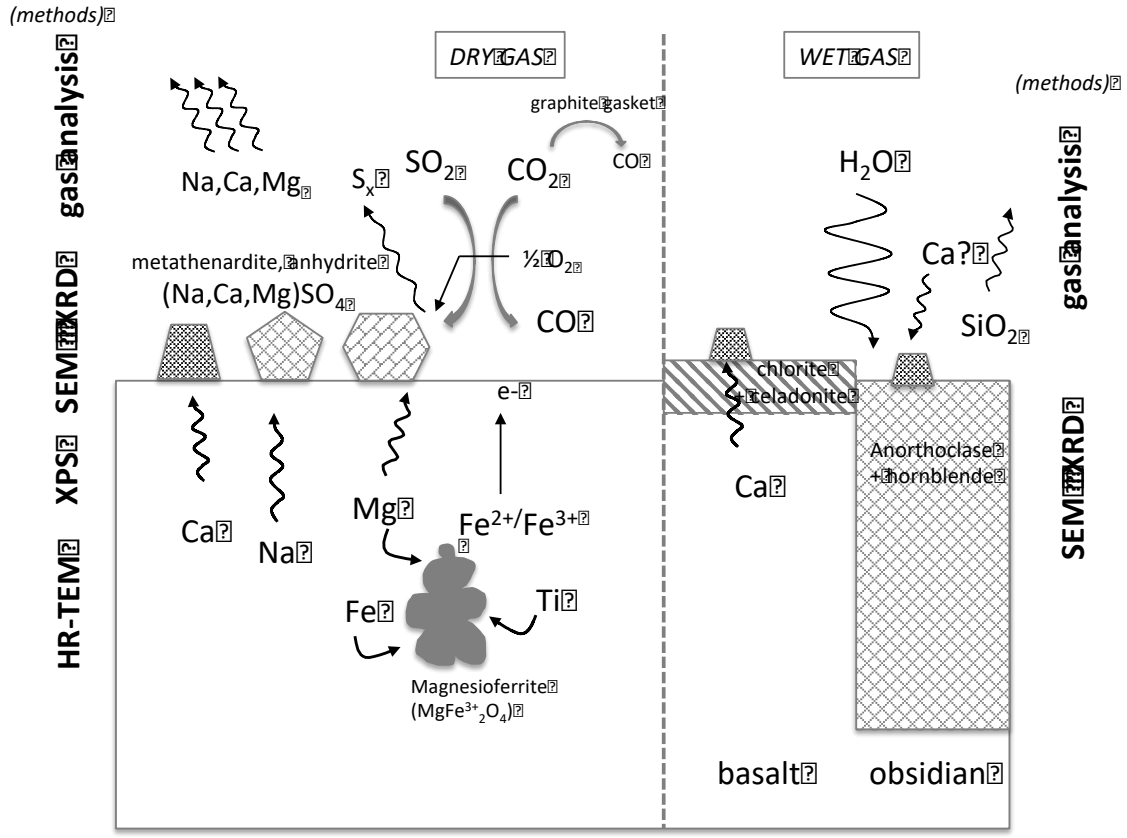

Figure 11: *General scheme depicting the chemical processes occurring at the gas-glass interface, inspired by Renggli and King (2018).*

4.3 Process and kinetics in wet gas

Addition of water to CO_2 or Venus-like gas drives spectacular changes. The olivine surface is covered by secondary or residual fibrous and massive material, the thickness of which being too small for a more detailed characterization. The most important changes were observed for the basalt glass and obsidian where a deeper alteration layer developed in few days, composed of anorthoclase + hornblende + iron oxides for obsidian and Ca,Na,Mg-sulfate + Fe,Mg-chlorites + celadonite for basalt glass (Fig. 11). In the latter case, celadonite, characterized by its 10Å reflection, is also clearly visible in the crushed bulk sample suggesting its presence below the surface. This zonation of alteration products is typical of hydrothermal alteration (Berger *et al.*, 2014). It is worth noting that under only few bars of water vapor the glass and olivine hydrolysis proceed to a similar manner than in condensed aqueous fluid, but obviously at a lower rate. The formation of OH-bearing phase in wet

gas, clays and amphibole, also raises the question of metastability of these phases in the present-day atmosphere regarding the general question of H_2O inventory of Venus. For amphibole, Straub and Burns (1993) proposed that Fe-poor oxyamphibole like hornblende should be stable under dry Venus conditions, unlike the thermodynamic prediction (Fegley and Treiman, 1992). Here, we tested the metastability of hydrous phase by reacting chlorite-type minerals in dry CO_2 (Fig. 3). We observed the dehydration of the clays (collapse of the interlayer equidistance) but not a true desorganisation (persistence of the reflections), hydroxyl groups being likely conserved. By contrast, an equivalent heating in oxidizing terrestrial conditions promotes the destruction of the structure, likely by oxidation of iron. This suggests that phyllosilicates may persist under present-day dry conditions provided the conditions are reducing enough to preserve the redox status of iron in the clay structure.

The most accurate observations were acquired on obsidian glass, that is likelynot a representative material of Venus's surface but is used hereas a proxy of alumino-silicates for a kinetic data processing. The high water pressure tested is out of range for the current Venus conditions but may be informative of early Venus or any early terrestrial planets such as Mars or the Earth. For Mars, the question of clay formation in its early history is addressed in Cannon *et al*. (2017).

The alteration kinetics of silicates depends on many factors influencing the chemistry or accessibility of the reaction interface. For glasses, the development of deep alteration layers is likely the first order parameter for long-time reaction (Berger *et al.*, 1994) even if metal rich nanometric surface layer also plays a significant role (Leturcq *et al.*, 1999). This last process may explain the higher alteration rate of obsidian (Fe-poor) when compared to basalt glass (Fe-rich). In the present study, the alteration in wet gas presents similar features with alteration in water at lower temperatures: non-linear dependence on time, $rate_{glasses} > rate_{olivine} > rate_{Cpx,plagioclase}$, hydrolysis of the silicate network by water (demonstrated by fH_2O dependence). The reaction kinetics in water is generally expressed through the framework of the Transition State Theory (TST) that postulates that the bulk rate is controlled by the decomposition of an activated complex at the mineral-solution interface. The dissolution rate, theoretically proportional to the Gibbs free energy change, may be more sophisticated when one considers the catalytic or inhibitor effect of electrolytes (Oelkers *et al.*, 1994), or several activated complexes (Berger *et al.*, 2002). However, the empirical application of TST to overall reaction is questioned by other approaches (Luttge, 2006; Pollet-Villard, 2016). Whatever the formalism, the observed rate law dependence on temperature generally follows an Arrhenius law, at least in the commonly applied 20-300°C temperature range. At higher temperatures, namely supercritical conditions, we postulate that the silicate alteration is still the result of a nucleophilic attack by the polarized water molecule. Thus, the overall rate is likely dependent on water density, as observed in our experiments. In other words, it is a function of the surface concentration of an activated complex formed by the network-forming oxides and the water molecules, according to Eq. 1 for the case of silica. In this equation we assume that one H_2O molecule generates two Si-OH group.

$$\equiv Si\text{-}O\text{-}Si\equiv + H_2O = 2\ \equiv Si\text{-}OH \qquad \text{Eq. (1)}$$

Considering rather a bulk dissolution reaction (still for silica), the balanced equation requires two water molecules for the entire dissolution according Eq. 2, and a complex order of reaction with respect to fH_2O is expected.

$$SiO_2 + 2\ H_2O = H_4SiO_4 \qquad \text{Eq. (2)}$$

Although our experiments were not designed in order to investigate detailed surface reactions, the empirical fit of the data presented in Fig 9b is consistent with a two-order reaction in most of fH_2O range. We distinguished three domains. At very low fH_2O, a threshold H_2O concentration seems required to initiate the reaction (no alteration in V12 and V14). Above this value and up to $fH_2O \approx 25$ MPa (i.e. 590 bar H_2O pressure), the data are well fitted by Eq. 3 which formalizes a two-order reaction.

$$y = 0.63\ fH_2O^2 \quad R^2 = 0.96 \quad \text{where } y \text{ is the altered layer thickness in mm} \qquad \text{Eq. (3)}$$

Under extreme water pressure, Eq. 3 underestimates the measured thickness. We attribute this discrepancy to the modification of the glass prior the recrystallization (Fig.8) suggesting another kinetic control. Note that in this kinetic approach we neglected a possible effect of the chemical affinity of reaction that we considered as being in a steady-state.

Alternatively to the previous TST-like model, we focused on the time-dependence of the shell thickness. The parabolic relationship between the obsidian alteration depth and the elapsed time (Fig. 9b) suggests a diffusion controlling process, likely through the altered layer. This effect may be taken into account with a shrinking-core formalism. A mathematical approach for describing coupled surface reaction and passivation is contained in the shrinking-core model developed in the catalysis literature (e.g. Wen, 1968). This model, initially developed for gas-solid interactions, combines the reaction rates at the reaction interface and the gas diffusion rates through the altered products. Initially, the reaction takes place at the outside surface of the particle, but as the reaction proceeds, the reacting surface will move inside, leaving beneath the product layer. It has been successfully used by White *et al.* (1994) to describe the topotactic transformation of magnetite to maghemite, for example. A more comprehensive review is available in King *et al.* (2018). In our case, assuming a classic first order of reaction and a high diffusion rate in gas outside the alteration layer, the altered layer thickness is related to time through an original expression given in Eq. (3). Derivation of this expression is given in the Appendix.

$$y = -\,D_A M/3\ k_S\,\rho + D_A C_{H2O} M/3\ \rho\sqrt{(1/(\ k_S\ C_{H2O})^2 + 6\ \rho t/D_A C_{H2O} M)} \qquad \text{Eq. (3)}$$

where y is the altered layer thickness in m, D_A the diffusion constant through the altered layer in m^2/s, t the elapsed time in s, C_{H2O} the concentration of gaseous reactant (here H_2O in mol/m^3), ρ is the density in kg/m^3, M the molar weight in mole SiO_2/m^3 and k_S the rate constant in $m/s/(mol_{H2O}/ m^3_{(g)})$.

D_A and k_S were estimated to be $1.1x10^{-13}$ $m^2.s^{-1}$ and $5.2x10^{-14}$ $m.s^{-1}$ ($mol_{H2O}.m_{(g)}^{-3}$), respectively, by regressing the data reported in Fig. 9b. The diffusion coefficient obtained here in the recrystallized rim is four orders of magnitude over than the diffusion coefficient of cations ($8.7x10^{-13}$ $cm^2.s^{-1}$ for Ca^{++}) in a rhyolitic glass at 800°C reported by Ayris *et al.* (2013). That means that in wet atmosphere the recrystallized rim progresses much faster than the ion diffusion and obliterates the chemical transfer in the glass (right box in Fig. 11). Note that k_s in the shrinking-core formalism, expressed in $m/s/(mol_{H2O}.m_{(g)}^{-3})$, cannot be compared to the rate constant in the TST, expressed in $mol.m^{-2}.s^{-1}$, because these constants are not based on the same definition. This is also reflected in their respective units. In a second step, the increase of altered layer thickness with C_{H2O} is modeled using the previous constants. The values of C_{H2O} and y for the 7 selected runs are reported in Table 5 with the parameters of the experiments.

Run	T (°C) ±3°C	duration (day)	$X(H_2O)$	P (bar)	H_2O (MPa)	C_{H2O} mol/m^3	y obs. (μm)	y meas. (μm)	ratio calc./meas.
V4	464	6	0.11	180-110	1.82	344	0	7.6	/
V3	470	6	0.50	218-115	8.44	218	72	31.9	0.44
V7	460	6	1	150	12.8	2900	75	38.7	0.52
V6	456	5	0.75	253-215	12.5	4781	62	47.7	0.77
V19	471	7	0.78	90-87	5.57	1125	35	22.1	0.63
V20	472	7	0.96	360-355	23.0	9937	350	92.2	0.26
V23	473	7	0.86	590	29.5	17500	1500	119	0.08

***Table 5**: Experimental conditions for selected H_2O bearing runs. The thickness of the recrystallized rim (y_{obs}) is compared to the value calculated by Eq.(3) and using the diffusion and rate constants deduced from three runs conducted at 90 bars during 1 day, one week and one month.*

The calculated values are in the order of the observed rim thickness except at low and high fH_2O. The low dielectric constant of the gas at low water pressure may explain the absence of network hydrolysis. At high pressure, the differences between the observed and calculated values may reflect an increase of the rate constant itself as mentioned before, promoted by the glass hydration as suggested by the observations (Fig. 8). In the intermediate range, such as the run conducted at the present day surface pressure (V19), the model is in reasonable agreement with the data.

5. Application to Venus and concluding remarks

The short duration of the experiments makes speculative the extrapolation to the geologic history of Venus. However, this current experimental study offers new insights to possible processes having

affected the surface of this planet, especially when addressing the matter of the contribution of vitreous material. Even if glasses are not considered as the most representative materials of Venus surface, they may have been produced in pyroclastic flow as those recently described in Campbell *et al.* (2017). In the case of differentiated volcanic rocks, the low water content of the Venus's crust inferred from isotopic studies (DeBergh *et al*., 1991; Donahue *et al.*, 1982) pleads for rhyolite lava instead of granitic magma (Johannes and Holtz, 1996). In addition, given the high atmospheric pressure in deep Venus atmosphere, the degassing process during volcanic eruption is likely partly impaired and as a consequence, the Venusian lava may even happen to be more enriched in volatile elements, i.e. in modifier elements promoting the vitrification, than their terrestrial counterparts (Swanson *et al.*, 1989; Gardner *et al.*, 1998; Hammer *et al.*, 1999).

In dry atmosphere, the alteration is tenuous. CO_2, as expected from its low dielectric constant, does not interact with the silicate framework and no secondary carbonates are observed. However, in the presence of SO_2 the oxidation of iron in glasses drives Ca, Na and Mg transfer to the surface, with formation of sulfate minerals, and even further into the gas. The elementary mechanisms established from our observations are finally close to the ones proposed by King *et al.* (2018) for pure SO_2-basalt glass interaction at low pressure and temperature over 600°C. Analysis of the sampled gas phase suggests that these elements, as well as silica, may precipitate at lower temperature. Extrapolation to Venus surface conditions and geologic time suggests that the colder zones at higher altitudes could likely act as the sink of Si, Ca, Na and Mg. This assumption may be correlated with the observed radar reflectivity anomalies at high elevation (see the review of Gilmore *et al.*, 2017), the best explanation of which being the presence of semiconductor-like material in the concerned area. Numerous suggestions were proposed in the literature (including rare substances in common geologic conditions such as Bi_2Te_3 or HgTe). Among them, Lazoryak *et al*. (2004) suggest that merrillite ($Ca_{18}Na_2Mg_2(PO_4)_{14}$) and whitlockite ($Ca_9(Mg, Fe^{++})(PO_4)_6(PO_3OH)$)) could have a ferroelectric behavior at Venus surface conditions. Our measurements best fit this assumption, even if the source of phosphorus is still to be discovered. We did not find, however, evidence of iron transfer into the gas phase, even if transfer from grain to grain is suspected. Olivine surfaces are also modified in dry atmosphere with the deposition of an iron oxide coating but without formation of enstatite or SiO_2(s) as suggested by some thermodynamic predictions. This process may be related to its chemical structure constituted to non-polymerized $[SiO_4]$ tetrahedrons linked with (mobile?) Mg and (immobile?) Fe. Some runs conducted with chlorite-type samples suggest that the clays may remain metastable in the dry Venus atmosphere provided that the conditions remain reducing enough to avoid the oxidation of iron. In all cases, the redox potential of the gas, allowing or not the oxidation of iron and SO_2, appears as a key in the Venus surface-atmosphere interaction. The disproportionation of sulfur as well as the CO/CO_2 redox reaction are two probable sources of oxygen.

When water is present in the atmosphere (early Venus or possibly modern (regional) volcanic activity) the wet gas causes mineral changes comparable to hydrothermal alteration on Earth, the

lower water activity of Venus atmosphere compensating the higher temperature. Obsidian recrystallizes into a mixture of plagioclase and amphibole while basaltic glass produced non-expandable clays minerals: chlorite-type (2:1:1) at the surface and likely celadonite (2:1) below the surface. Basically, the alteration process appears to be more isochemical than in dry gas. It is also worth pointing out the absence of secondary carbonate even in the pure H_2O-CO_2 system. This observation is consistent with the experimental results of Fabre *et al.* (2011; 2013) at lower temperature in the context of snowball Earth aftermath. They showed that the abiotic precipitation of carbonates requires a complex hydrologic regime, i.e. a sustainable water body, which is unlikely in our Venusian context, even on Early Venus. However these mechanisms were established from data obtained with a rhyolitic glass (obsidian). In the case of basalt glass, most likely for Venus, our data were not sufficient to detail the processes and rates in wet atmosphere but our observations suggest a slower and different reaction. The altered rim was not recrystallized similar to the obsidian. We only observed a chemically modified layer for the run using the higher H_2O pressure (Fig. 8a). This may be due to the higher Fe content in the basalt glass, compared to obsidian, which promotes the formation of a surface passive layer. Consequently, its alteration process is more likely controlled by diffusion rather than by surface hydrolysis. An accurate evaluation of the alteration rate of basalt glass under early Venus conditions needs much longer and challenging experiments.

Based on our observation on obsidian alteration, used here as a proxy of aluminosilicates, we propose a kinetic model by considering either an empiric correction term between Earth and Venus short time processes or a shrinking-core equation that better models the long term reactions. For the short time scale processes, the lower fH_2O compensates the higher temperature when compared to condensed water at lower temperature. As an example, for 9 MPa H_2O (a volcanic vapor jet under current conditions) the alteration kinetics is roughly 30 times lower than a simple extrapolation of rates established in condensed water at lower temperature, and consequently is so roughly equivalent to an alteration process at 300°C at the earth surface using an activation energy of 60kJ/mol. By contrast, olivine crystals in the picritic basalt exposed to 590 bars H_2O-rich fluid (V23, Table 3) did not show a visible alteration layer after one week despite of the high fH_2O. We exclude a thermodynamic equilibrium with the fluid at this temperature but a passivation effect by secondary iron oxy-hydroxides at the olivine surface may be envisaged as suggested by Sissmann *et al.* (2013). The thickness, and likely the composition, of this possible protective layer is different from the iron oxide coating developed under dry composition. This suggests another active mechanism: hydroxide precipitation or less Si and Mg degassing?

Thanks to our shrinking-core based model, we can evaluate the lifetime of the dust and particles constituting the Venusian regolith. We established a relationship between the water vapor pressure, the particles size and the conversion time of the particle, i.e. the required time for the complete reaction. The results reported in Figure 12 suggest that the lifetime of vitreous dust or fine grain material should be limited with quite a short geologic time scale, if ever produced. For example, using arbitrarily a

vapor pressure equivalent to the present deep atmosphere pressure (gray bar in Figure 12), the lifetime of millimeter particles does not exceed one year. At 5 bar H_2O in 90 bar CO_2, near the suspected threshold limit of water influence in our experiments, the lifetime of the same particle raises to 10 years.

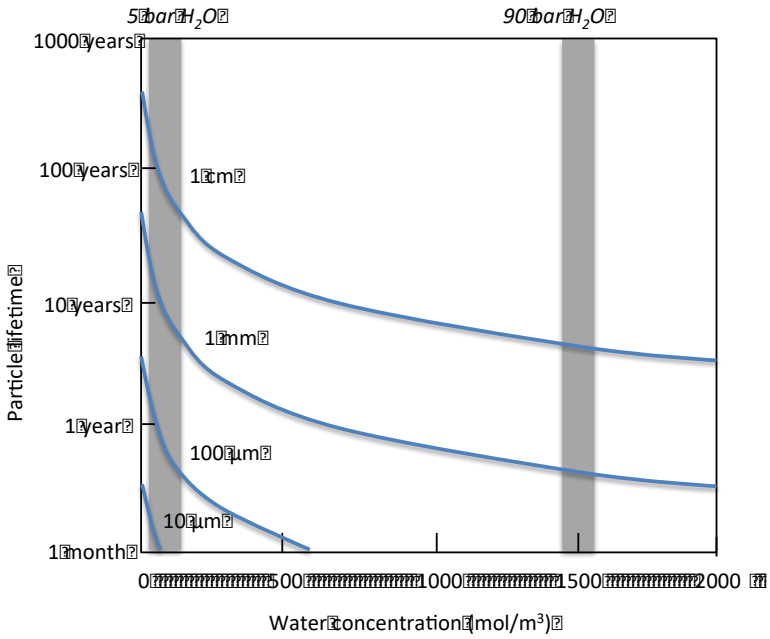

Figure 12: *Lifetime of glass particles as a function of size and water content in the atmosphere. The correspondence between pressure and water concentration were calculated by EOS.*

Finally, the present inventory of possible reactions affecting, or having affected, the Venus surface offers an interesting insight on mineralogical and chemical changes of the Venus surface. In particular, it is likely that early Venus was above the runaway greenhouse limit (Zahnle, 2006) and did not have a sustainable water body making the processes investigated here of primary importance for its geological history. In addition, the *in-situ* surface analyses that could be performed in future missions may be affected by the weathering processes, including in dry atmosphere, as discussed in this paper.

Aknowledgements

The bulk chemical analyses of the experimental materials were performed in the frame of the National Facilities of the Centre de Recherches Pétrographiques et Géochimiques (Nancy, France), and the FIB/MET analyses in Raimond Castaing Center of Microanalytical technique (Toulouse, France). The long-term acquisition of *in-situ* XRD pattern on the polished section (Fig. 2) was performed by B. Lanson, ISTerre/OSUG (Grenoble, France). We would like to thank Frédéric Candaudap (GET, OMP, Toulouse) for his assistance with the MS-ICPM analysis and Serge Chevrel (IRAP, Toulouse) for their helpful scientific discussions. The manuscript was clearly improved based on the comments and remarks made by D. Daval and an anonymous reviewer.

References

AGUERO, A., M. GUTIÉRREZ, L. KORCAKOVA, T. T. M. NGUYEN, B. HINNEMANN and S. SAADI 2011. Metal dusting protective coatings. A literature review. *Oxid. Met.* **76**, 23-42.

AVELINE, D. C., W. J. ABBEY, M. CHOUKROUN, A. H. TREIMAN, M. D. DYAR, S. E. SMREKAR and S. M. FELDMAN 2011. Rock and mineral weathering experiments under model Venus conditions. *LPS Conf.* XXXXII, #2165

AYRIS, P. M., A. F. LEE, K. WILSON, U. KUEPPERS, D. B. DINGWELL and P. DELMELLE 2013. SO_2 sequestration in large volcanic eruptions: High-temperature scavenging by tephra. *Geochim. Cosmochim. Acta* **110**, 58-69.

BAKKER, R. J. 2009. Package FLUIDS. Part 3: Correlations between equations of state, thermodynamics and fluid inclusions, *Geofluids* **9**, 63–74. doi:10.1111/j.1468-8123.2009. 00240.x.

BERGER, G., C. CLAPAROLS, C. GUY and V. DAUX 1994. Dissolution rate of a basalt glass in silica-rich solutions: implications for long-term alteration. *Geochim. Cosmochim. Acta* **58**, 4875-4886.

BERGER, G., D. BEAUFORT and J.-C. LACHARPAGNE 2002. Experimental dissolution of sanidine under hydrothermal conditions: mechanism and rate. *Amer J. Sci.* **302**, 663-685.

BERGER, G. and T. AIGOUY 2011. Experimental rocks alteration under venus-like conditions. *LPS Conf. XXXXII*, # 1660.

BERGER, G., MEUNIER A. and D. BEAUFORT 2014. Clay minerals forming on Mars: the possible contribution of basalt out-gassing. *Planet. Space Sci.* **95**, 25-32. doi/10.1016/j.pss.2013.05.024

BERGER, G., D. BEAUFORT and R. ANTOINE 2018. Clay minerals related to the late magmatic activity of the Piton des Neiges (Réunion island). Consequence for the primitive crusts. *Clay minerals*, 1-34. 10.1180/clm.2018.51.

CAMPBELL, B. A., G. A. MORGAN, J. L. WHITTEN, L. M. CARTER, L. S. GLAZE and D.B . CAMPBELL 2017. Pyroclastic flow deposits on Venus as indicators of renewed magmatic activity. *J. Geophys. Res.: Planets* **122**, 1580-1596.

CANNON, K. M., S. PARMAN and J. MUSTARD 2016. Primordial clays on Mars formed beneath a steam or supercritical atmosphere. *Nature* **552**, 24657.

CAPOBIANCO, R. M., M. S. GRUSZKIEWICZ, R. J. BODNAR and J. D. RIMSTIDT 2015. Conductivity measurements on H_2O-bearing CO_2-rich fluids. *J. Sol. Chem.* **44**, 934–962.

COOK, G. B. and R. F. COOPER 1990. Chemical diffusion and crystalline nucleation during oxidation of ferrous iron-bearing magnesium aluminosilicate glass. *J. Non-Crystalline Solids* **120**, 207-222.

COOPER, R. F., J. B. FANSELOW and D. B. POKER 1996. The mechanism of oxidation of a basaltic glass: Chemical diffusion of network-modifying cations. *Geochim. Cosmochim. Acta* **60**, 3253-3265.

DAVAL, D., I. MARTINEZ, J. CORVISIER, N. FINDLING, B. GOFFÉ and F. GUYOT 2009. Carbonation of Ca-bearing silicates, the case of wollastonite: Experimental investigations and kinetic modeling. *Chemical Geology* **265**, 63-78.

DEBERGH, C., B. BEZARD, T. OWEN, D. CRISP, J.-P. MAILLARD, and B. L. LUTZ 1991. Deuterium on Venus: Observation from Earth, *Science* **251**, 547– 549.

DELMELLE, P., F. B. WADSWORTH, E. C. MATERS and P. M. AYRIS 2018. High temperature reactions between gases and ash particles in volcanic eruption plumes. *Reviews in Mineralogy & Geochemistry* **84**, 295-308.

DONAHUE, T. M., J. H. HOFFMAN, R. R. HODGES JR., and A. J. WATSON 1982. Venus was wet: A measurement of the ratio of D to H. *Science* **216**, 630– 633.

DUAN, Z., N. MØLLER and J. H. WEARE 1995. Equation of state for the NaCl-H_2O-CO_2 system: prediction of phase equilibria and volumetric properties. *Geochim. Cosmochim. Acta* **59**, 2869-2882. doi:10.1016/0016-7037(95)00182-4.

EKONOMOV, A. P., Y. GOLOVIN and B. E. MOSHKIN 1980. Visible radiation observed near the surface of Venus - Results and their interpretation. *Icarus* **41**, 65-75.

FABRE, S., G. BERGER and A. NÉDÉLEC 2011. Modeling of continental weathering under high-CO_2 atmospheres during Precambrian times. *G-cubed* **12**, doi:10.1029/2010GC003444.

FABRE, S., G. BERGER, V. CHAVAGNAC and Ph. BESSON 2013. Cap carbonates origin: the experimental approach. *Paleo3* **392**, 524-533.

FARELAS, F., Y. S., CHOI and S. NEŠIĆ 2013. Corrosion behavior of API 5L X65 carbon steel under supercritical and liquid carbon dioxide phases in the presence of water and sulfur dioxide. *Corrosion* **69**, 243-250.

FEGLEY Jr., B. and A.H. TREIMAN 1992. Chemistry of atmosphere-surface interactions on Venus and Mars, in *Venus and Mars: Atmospheres, Ionospheresand Solar Wind Interactions*, edited by Luhmann, J.G., Tatrallyay, M., Pepin, R.O., *AGU Geophys. Monograph* **66**, 7-71.

FEGLEY Jr., B. and R.G. PRINN 1989. Estimation of the rate of volcanism on Venus from reaction rate measurements. *Nature* **337**, 55-58.

FEGLEY, B. JR., G. KLINGELHÖEFER, R. A. BRACKETT, N. IZENBERG, D. T. KREMSER and K. LODDERS 1995. Basalt oxidation and the formation of hematite on the surface of Venus. *Icarus* **118**, 373-383.

FEGLEY, B. JR., M. Y. ZOLOTOV, K. and LODDERS 1997. The oxidation state of the lower atmosphere and surface of Venus. *Icarus* **125,** 416-439.

GARDNER, C. A., K.V. CASHMAN and C. A. NEAL 1998. Tephra-fall deposits from the 1992 eruption of Crater Peak, Alaska: implications of clast textures for eruptive processes. *Bulletin of Volcanology* **59**, 537–555. https://doi.org/10.1007/s004450050208

GILMORE, M., A. TREIMAN, J. HELBERT and S. SMREKAR 2017. Venus Surface Composition constrained by observation and experiment. *Space Sci. Rev.* **212**, 1511-1540. DOI 10.1007/s11214-017-0370-8.

HAMMER, J. E., K. V. CASHMAN, R. P. HOBLITT, and S. NEWMAN 1999. Degassing and microlite crystallization during pre-climactic events of the 1991 eruption of Mt. Pinatubo, Philippines. *Bulletin of Volcanology* **60**, 355-380. https://doi.org/10.1007/s004450050238

HASHIMOTO, G. L., M. ROOS-SEROTE, S. SUGITA, M. S. GILMORE, L. W. KAMP, R. W. CARLSON, and K. H. BAINES 2008. Felsic highland crust on Venus suggested by Galileo Near-Infrared Mapping Spectrometer data. *J. Geophys. Research* **113**, E00B24.

JACQUEMET, N., J. PIRONON and J. SAINT-MARC 2008. Mineralogical changes of a well cement in various H_2S-CO_2(-brine) fluids at high pressure and temperature. *Environ. Sci. Technol.* **42**, 282-288. doi:10. 1021/es070853s.

JOHANNES, W. and F. HOLTZ 1996. Petrogenesis and experimental petrology of granitic rocks. Springer, Berlin, 335 p.

KING P. L., V. W. WHEELER, C.J. RENGGLI, A. B., PALM, S. A. WILSON, A. L. HARRISON, B. MORGAN, H. NEKVASIL, U. TROITZSCH, T. MERNAGH, L. YUE, A. BAYON, N. J. DIFRANCESCO, R. BALIE, P. KREIDER and W. LIPINSKI 2018. Gas-solid reactions: Theory, experiments and case studies relevant to earth and planetary processes. *Reviews in Mineralogy & Geochemistry* **84**,1-56.

KWON, Y. J. and G. A. MANSOORI 1993. Solubility modeling of solids in supercritical fluids using the Kirkwood-Buff fluctuation integral with the Hard-Sphere expansion theory. *The J. Supercrit. Fluids* **6**, 173-180.

LASAGA, A. C. and A. LÜTTGE 2001. Variation of crystal dissolution rate based on a dissolution stepwave model. *Science* **291**, 2400-2404.

LAZORYAK, B. I., V.A. MOROZOV, A. A. BELIK, S. YU. STEFANOVICH, V. V. GREBENEV, I. A. LEONIDOV, E. B. MITBERGE, S. A. DAVYDOV, O. I. LEBEDEV and G. VAN TENDELOO 2004. Ferroelectric phase transition in the whitlockite-type $Ca_9Fe(PO_4)_7$; crystal structure of the paraelectric phase at 923 K. *Solid State Sci.* **6**, 185-195.

LETURCQ, G., G. BERGER, T. ADVOCAT and E. VERNAZ 1999. Initial and long-term dissolution rates of aluminosilicate glasses enriched in Ti, Zr and Nd. *Chem. Geol.* **160**, 39-62.

LUTTGE, A. 2006. Crystal dissolution kinetics and Gibbs free energy. *Journal of Electron Spectroscopy and Related Phenomena* **150**, 248-259.

MARCQ, E., B. BE ZARD, P. DROSSART, G. PICCIONI, J. M. REESS, and F. HENRY 2008. A latitudinal survey of CO, OCS, H_2O, and SO_2 in the lower atmosphere of Venus: Spectroscopic studies using VIRTIS-H. *J. Geophys. Res.* **113**, E00B07. doi:10.1029/2008JE003074.

OELKERS, E. H., J. SCHOTT and J.-L. DEVIDAL 1994. The effect of aluminum, pH, and chemical affinity on the rates of aluminosilicate dissolution reactions. *Geochim. Cosmochim. Acta* **58**, 2011-2024.

PALM, A.B., KING ,P.L., RENGGLI, C.J., HERVIG, R.L., DALBY, K.N., HERRING, .A., MERNAGH, T.P., EGGINS, S.M., TROITZSCH, U., BEECHING, L., KINLEY, L. and GUAGLIARDO, P. (2018) Unravelling the consequences of SO_2-basalt reactions for geochemical fractionation and mineral formation. *Reviews in Mineralogy & Geochemistry* **84**, 257-283.

PEARCE, J.K., A.C.K. LAW, G.K.W. DAWSON and S.D. GOLDING 2015. SO_2-CO_2 and pure CO_2 reactivity of ferroan carbonates at carbon storage conditions. *Chem. Geol.* **411**, 112-124.

PEARCE, J. K., G. K. W. DAWSON, A. C. K. LAW, D. BIDDLE and S.D. GOLDING 2016. Reactivity of micas and cap-rock in wet supercritical CO_2 with SO_2 and O_2 at CO_2 storage conditions. *Applied Geochem.* **72**, 59-76. doi:10.1016/j.apgeochem.2016.06.010

PIETERS, C. M., J. W. HEAD, W. PATTERSON, J. GARVIN, V. L. BARSUKOV, A. T. BASILEVSKY, I.L. KHODAKOVSKY, A. S. SELIVANOV, A. S. PANFILOV, Y.M. GEKTIN and Y. M. NARAYEVA 1986. The color of the surface of Venus. *Science* **234**, 1379-1383.

PLYASUNOV, A.V. 2011. Thermodynamic properties of H_4SiO_4 in the ideal gas state as evaluated from experimental data. *Geochim. Cosmochim. Acta* **75**, 3853-3865. doi:10.1016/j.gca.2011.04.016

POLLET-VILLARD, M., D. DAVAL, P. ACKERER, G.D. SALDI, B. WILD, K.G. KNAUSS and B. FRITZ 2016. Does

crystallographic anisotropy prevent the conventional treatment of aqueous mineral reactivity? A case study based on K-feldspar dissolution kinetics. *Geochim. Cosmochim. Acta* **190**, 294-308.

RADOMAN-SHAW, B. G., R. P. HARVEY, G. C. C. COSTA, N. S. JACOBSON, A. AVISHAI and L.M. NAKLEY 2017. The stability of calcium silicates and calcium carbonate on the surface of Venus. *LPS Conf. XLVIII*, # 2701.

REGNAULT, O., V. LAGNEAU and H. SCHNEIDER 2009. Experimental measurement of portlandite carbonation kinetics with supercritical CO_2. *Chem. Geol.* **265**, 113-121. doi:10.1016/j.chemgeo.2009.03.019

RENGGLI , C.J. and P. L. KING 2018. SO_2 gas reactions with silicate glasses. *Reviews in Mineralogy & Geochemistry* **84**, 229-255.

SAUTTER V., M. TOPLIS, R. C.WIENS, A. COUSIN, C. FABRE, O. GASNAULT, S. MAURICE, O. FORNI *et al.* 2015. In situ evidence for continental crust on early Mars. *Nature Geoscience* **8**, 605-609.

SAVARY, V., G. BERGER, M. DUBOIS, J.C. LACHARPAGNE, A. PAGES, S. THIBEAU and L. LESCANNE 2012. The Solubility of CO_2 + H_2S Mixtures in Water and 2 M NaCl at 120 °C and Pressures up to 35 MPa. *Inter. J. Greenhouse Gas Control* **10**, 123-133.

SCHAEF, H. T., B. P. MCGRAIL and A. T. OWEN 2009. Basalt-CO_2-H_2O Interactions and variability in carbonate mineralization rates. *Energy Procedia* **1**, 4899-4906.

SCHAEF, H. T., C. F. WINDISCH JR., B. P. MCGRAIL, P. F. MARTIN and K. M. ROSSO 2011. Brucite [$Mg(OH_2)$] carbonation in wet supercritical CO_2: An in situ high pressure X-ray diffraction study. *Geochim. Cosmochim. Acta* **75**, 7458-7471. doi:10.1016/j.gca.2011.09.029

SHKURATOV, Y. G, M. A. KRESLAVSKY and O. V. NIKOLAYEVA 1987. Albedo-color diagram of the Venusian surface and its interpretation. *Solar System Research* **21**, 94-102.

SIMAKIN, A.G., T. P. SALOVA, R. I. GABITOV and S. I. ISAENKO 2016. Dry CO_2-CO fluid as an important potential Deep Earth solvent. *Geofluids* **16**, 1043-1057. DOI: 10.1111/gfl.12204

SISSMANN, O., D.DAVAL, F.BRUNET, F.GUYOT, A.VERLAGUET, Y.PINQUIER, N.FINDLING, and I. MARTINEZ 2013. The deleterious effect of secondary phases on olivine carbonation yield : Insight from time-resolved aqueous-fluid sampling and FIB-TEM characterization. *Chemical Geology* **357**, 186-202.

SMREKAR, S.E. and C. SOTIN 2012. Constraints on mantle plumes on Venus: implications for volatile history. *Icarus* **217**, 510-523.

SOUCHON, A. L., P. C. PINET, S. D. CHEVREL, Y. H. DAYDOU, D. BARATOUX, K. KURITA, M. K. SHEPARD and P. HELFENSTEIN 2011. An experimental study of Hapke's modeling of natural granular surface samples. *Icarus* **215**, 313-331.

STRAUB, D.W. and R.G. BURNS 1991. Degradation of Fe-Mg silicates in hot CO_2 atmospheres: Applications to Venus, *LPS Conf.* XXII, 1349-1350.

SURKOV, Y. A., V. L. BARSUKOV, L. P. MOSKALYEVA, V. P. KHARYUKOVA and A. L. KEMURDZHIAN 1984. New data on the composition, structure, and properties of Venus rock obtained by Venera-13 and Venera-14. *J. Geoph. Research* **89**, 393-402.

SURKOV, Y. A., F. F. KIRNOZOV, V. N. GLAZOV, A. G. DUNCHENKO, L. P. TATSY and O. P. SOBORNOV 1987. Uranium, thorium, and potassium in the Venusian rocks at the landing sites of Vega-1 and Vega-2. *J. Geoph. Research* **92**, 537-540.

SURKOV, Y. A., L. P. MOSKALYOVA, V. P. KHARYUKOVA, A. D. DUDIN, G. G. SMIRNOV and S. ZAITSEVA 1986. Venus rock composition at the Vega-2 landing site. *J. Geoph. Research* **91,** 215-218.

SWANSON, S.E., M.T. NANEY, H.R. WESTRICH and J.C. EICHELBERGER 1989. Crystallization history of Obsidian Dome, Inyo Domes, California. *Bulletin of Volcanology* **51**, 161–176. https://doi.org/10.1007/BF01067953

TAYLOR, F.W., H. SVEDHEM and J.W. HEAD 2018. Venus: the atmosphere, climate, surface, interior and near-space environment of an Earth-like planet. *Space Science Review* **214**, 35.

TU, R. and T. GOTO 2005. Corrosion behavior of Hastelloy-XR alloy in O_2 and SO_2 atmosphere. *Materials Transactions* **46**, 1882-1889.

WEI, L., X. PANG and K. GAO 2016. Effect of small amount of H_2S on the corrosion behavior of carbon steel in the dynamic supercritical CO_2 environments. *Corrosion Science* **103**, 132-144.

WEN, C.Y. 1968. Noncatalytic heterogeneous solid-fluid reaction models. *Industrial & Engineering Chemistry* **60**, 34–54.

WHITE, A.F., M.L. PETERSON and J., M.F. HOCHELLA 1994. Electrochemistry and dissolution kinetics of magnetite and ilmenite. *Geochim. Cosmochim. Acta* **58**, 1859–1875.

ZAHNE, K.J. 2006. Earth's Earliest Atmosphere. *Elements* **2**, 217-222.

ZHANG, R., S. HU and X. ZHANG 2011. Dissolution rates of silicate minerals in water from a subcritical to a supercritical state: effect of solvent properties. *Res. Chem. Intermed.* **37**, 243-258.

ZHANG, R., X. ZHANG and S. HU 2015. Basalt–water interactions at high temperatures: 1. Dissolution kinetic experiments of basalt in water and NaCl-H_2O at temperatures up to 400°C, 23 MPa and implications. *Journal of Asian Earth Science.* **110**. 10.1016/j.jseaes.2015.03.042.

ZOLOTOV, M. Y., B. FEGLEY JR. and K. LODDERS 1997. Hydrous silicates and water on Venus. *Icarus* **130**, 475-494.

ZOLOTOV, M. Y. 2018. Gas–solid interactions on Venus and other solar system bodies. *Reviews in Mineralogy & Geochemistry* **84**, 351-392.